

# Experimentally Induced Retinal Projections to the Ferret Auditory Thalamus: Development of Clustered Eye-Specific Patterns in a Novel Target

Alessandra Angelucci, Francisco Clascá, Emanuela Bricolo, Karina S. Cramer, and Mriganka Sur

*Department of Brain and Cognitive Sciences, Massachusetts Institute of Technology, Cambridge, Massachusetts 02139*

We have examined the relative role of afferents and targets in pattern formation using a novel preparation, in which retinal projections in ferrets are induced to innervate the medial geniculate nucleus (MGN). We find that retinal projections to the MGN are arranged in scattered clusters. Clusters arising from the ipsilateral eye are frequently adjacent to, but spatially segregated from, clusters arising from the contralateral eye. Both clustering and eye-specific segregation in the MGN arise as a refinement of initially diffuse and overlapped projections. The shape, size, and orientation of retinal terminal clusters in the MGN closely match those of relay cell dendrites arrayed within fibrodendritic laminae in the MGN. We conclude that specific aspects of a projection system are regulated by afferents and others by targets. Clustering of retinal projections within the

MGN and eye-specific segregation involve progressive remodeling of retinal axon arbors, over a time period that closely parallels pattern formation by retinal afferents within their normal target, the lateral geniculate nucleus (LGN). Thus, afferent-driven mechanisms are implicated in these events. However, the termination zones are aligned within the normal cellular organization of the MGN, which does not differentiate into eye-specific cell layers similar to the LGN. Thus, target-driven mechanisms are implicated in lamina formation and cellular differentiation.

*Key words: retinogeniculate; eye-specific segregation; cholera toxin subunit B; medial geniculate nucleus; afferents; cross-modal plasticity*

A fundamental feature of the development of the mammalian brain is the formation of patterned terminations in a target structure by afferents from a source structure. Some of the best studied examples of developmental pattern formation exist in the visual pathway of higher mammals. In ferrets, for example, retinal axons from the two eyes terminate in eye-specific layers in the lateral geniculate nucleus (LGN; Linden et al., 1981), and axons of on-center and off-center retinal ganglion cells from each eye subsequently form on and off sublayers within eye-specific layers (Hahm et al., 1991). Further along in the visual pathway, axons from eye-specific layers of the LGN terminate in ocular dominance columns in primary visual cortex (Law et al., 1988), whereas axons of on-center and off-center LGN cells terminate in contrast dominance columns within eye-specific columns (Zahs and Stryker, 1988). Several lines of evidence indicate that the formation of both retinogeniculate and geniculocortical termination patterns relies on afferent as well as target influences during development (for review, see Shatz, 1990; Cramer and Sur, 1995).

An issue that remains unresolved is the relative role of afferent and target structures in different aspects of pattern formation. Manipulating afferent activity in the visual pathway, for example by intraocular injection of tetrodotoxin or by lid suture, alters termination patterns in both the retinogeniculate and geniculo-

cortical projections (Stryker and Harris, 1986; Cramer and Sur, 1997). Similarly, early removal of retinal input by prenatal monocular enucleation affects LGN lamination and individual retinogeniculate axon arbors from the remaining eye (Garraghty et al., 1988a,b). However, such manipulations invariably affect target activity as well. Manipulating target activity alone, for example by infusion of antagonists to NMDA receptors, alters retinogeniculate on/off but not eye-specific termination patterns (Hahm et al., 1991; Smetters et al., 1994), as well as developmental plasticity of eye-specific projections in cortex (Bear et al., 1990; compare Hata and Stryker, 1994). Together, these studies indicate a complex and not easily separable interplay between afferent axons and target cells in shaping visual projection patterns. Furthermore, within the retinogeniculate pathway, retinal axon arbors are initially widespread but are progressively constrained to form focal arbors that lie within cellular layers and sublayers of the LGN; the layers are themselves separated by cell poor interlaminar spaces. Restriction of arbors and formation of cellular layers occur nearly simultaneously in retinogeniculate development (Linden et al., 1981; Hahm et al., 1991), leaving open the issue of whether afferents induce differentiation of targets or vice versa.

We have examined several of these issues in a novel preparation, in which retinal projections in ferrets are induced to innervate the medial geniculate nucleus (MGN). Specifically, we asked whether projections from the two eyes initially overlap in “re-wired” ferrets and subsequently segregate into eye-specific regions even within a novel target, the MGN, as they do in their normal target, the LGN. Such a finding would constitute important evidence for afferent regulation of eye-specific segregation. If projections from the two eyes do segregate, do they form eye-specific layers, and does the MGN differentiate into layers with interlaminar spaces? Such a finding would demonstrate afferent

Received Oct. 3, 1996; revised Dec. 23, 1996; accepted Jan. 3, 1997.

This research was supported by grants from National Institutes of Health and the March of Dimes (M.S.) and a Fogarty International Fellowship (F.C.). We thank S. Kuffler for technical assistance, Jitendra Sharma for help with figures, Dr. R. P. Marini for assistance with surgical procedures, and Peter Dayan for helpful comments on this manuscript.

Correspondence should be addressed to Dr. Mriganka Sur, Department of Brain and Cognitive Sciences, Massachusetts Institute of Technology, E25-235, 45 Carleton Street, Cambridge, MA 02139.

Copyright © 1997 Society for Neuroscience 0270-6474/97/172040-16\$05.00/0

**Table 1. Intraocular injections in adult rewired ferrets**

| Case    | Lesioned hemisphere/s | Eye(s) injected with CTB | Eye injected with WGA-HRP |
|---------|-----------------------|--------------------------|---------------------------|
| F94-82  | Left                  | Right                    |                           |
| F94-85  | Left                  | Both                     |                           |
| F94-89  | Both                  | Both                     |                           |
| F94-97  | Both                  | Right                    | Left                      |
| F94-146 | Left                  | Left                     |                           |
| F94-178 | Right                 | Right                    |                           |
| F94-212 | Left                  | Both                     |                           |
| F94-251 | Both                  | Left                     |                           |
| F94-252 | Both                  | Left                     |                           |
| F95-5   | Both                  | Left                     |                           |
| F95-75  | Both                  | Right                    | Left                      |
| F95-92  | Both                  | Right                    |                           |
| F95-93  | Both                  | Right                    |                           |

regulation of target differentiation. Conversely, do eye-specific terminations align themselves with the cellular organization of the MGN rather than create distinct eye-specific layers? Such a finding would demonstrate target regulation of afferent arbor location. We find that retinal terminations in the MGN of rewired ferrets do segregate into eye-specific regions, but that the termination zones are aligned with the intrinsic cellular organization of the MGN rather than organized into separate eye-specific layers. These data provide clear evidence for afferent and target regulation of specific aspects of development of a projection system.

Parts of this work have been reported previously in abstract form (Angelucci et al., 1994, 1995, 1996a).

## MATERIALS AND METHODS

**Animals.** The animals used in the present study were pigmented ferrets (*Mustela putorius furo*; family Mustelidae, order Carnivora) bred in our colony or purchased from Marshall Farms (North Rose, NY). Gestation time was  $41 \pm 1$  d. The day of birth was designated postnatal day (P) 0. A total of 13 adult (Table 1) and 24 young postnatal (Table 2) ferrets were used. Most of these animals ( $n = 33$ ) received neonatal brain lesions to reroute retinal axons to the auditory thalamus. Some normal controls ( $n = 4$ ) were included for comparison. Throughout this study we refer to the operated animals as rewired ferrets.

**Neonatal surgery.** The surgical protocol used in this study to reroute retinal fibers to the MGN is a modification of that reported previously from this laboratory (Sur et al., 1988; Pallas et al., 1994). One day after birth, ferret pups were anesthetized by hypothermia. Under sterile conditions and microscopic observation, the scalp was incised along the sagittal midline. A small craniotomy was made in the soft occipital bone overlying the posterior cerebral fossa, exposing the mesencephalon. To ablate the ascending ipsilateral auditory pathways to the MGN, the lateral third of the mesencephalon was coronally sectioned at the mid-collicular level. This lateral cut transected the brachium of the inferior colliculus (BIC) but extended medial and ventral to it to include extrabrachial inputs to the MGN. The latter consist of inputs from the ipsilateral nuclei of the lateral lemniscus and the nucleus of the BIC that course ventrally and medially to the BIC, respectively (Angelucci, 1996). The intercollicular commissure was cauterized to sever the contralateral auditory inputs to MGN, and both the superficial and deep layers of the superior colliculus (SC) were ablated on the same side of the deafferented MGN. In some cases, both inferior colliculi (IC) were also cauterized. A few animals were operated only on one side of the brain ( $n = 5$ ; Table 1). In the remaining animals, the set of lesions described above was performed bilaterally. On completion of surgery, the wound was closed with reabsorbable 5-0 suture. The pups were revived under a heat lamp, returned to the jill, and monitored until time of intraocular injections.

**Intraocular injections of tracers and staining procedures.** Adult animals were anesthetized with ketamine (30 mg/kg, i.m.) and xylazine (1.5 mg/kg, i.m.). Between the ages of P12 and P27, only ketamine (40 mg/kg) was

administered, whereas pups younger than P12 were anesthetized by deep hypothermia.

A first group of adult rewired ferrets received injections of cholera toxin subunit B (CTB) into the vitreal chamber of one or both eyes ( $n = 11$ ; Table 1). Procedures for CTB injections and immunohistochemical staining have been described in detail elsewhere (Angelucci et al., 1996b). Briefly, under general and local anesthesia, 10  $\mu$ l of a 1% solution of CTB (Low salt; List Biological Labs, Campbell, CA) in distilled water was injected into the vitreal chamber. The animals were allowed to survive for 3–6 days, euthanized with sodium pentobarbital (80 mg/kg, i.p.), and transcardially perfused with saline, followed by 4% paraformaldehyde in 0.1 M phosphate buffer (PB), pH 7.4, for 30 min. The brains were then blocked stereotaxically, removed from the skull, post-fixed overnight in the same fixative, and cryoprotected by soaking in 30% phosphate buffered sucrose for 1–2 days before sectioning with a freezing microtome. Serial 40- $\mu$ m-thick coronal sections were collected. Two brains (F95–92 and F95–93; Table 1) were sectioned in the parasagittal and horizontal planes, respectively. Alternate sections were pretreated in 0.3%  $H_2O_2$  and then in glycine (0.1 M) in 0.1 M PBS, pH 7.4. To block nonspecific binding sites, sections were preincubated overnight at 4°C in 4–5% normal rabbit serum (NRS), 2.5% BSA, and 0.3–0.5% Triton X-100 in PBS. Immunostaining was carried out by incubating the sections first in goat anti-CTB (List Biological Labs; 1:4000 with 2% Triton X-100, for 2 d at room temperature), then in biotinylated rabbit anti-goat IgG (Vector Laboratories, Burlingame, CA; 1:200 with 1% Triton X-100, for 1 hr), subsequently in ABC (Vectastain Elite, Vector Laboratories; 1:100, for 1 hr), and finally developed with a  $CoCl_2$ -enhanced DAB (Sigma, St. Louis, MO) reaction, or with Vector VIP substrate (Vector Laboratories). For cytoarchitectonic identification of the thalamic nuclei and MGN subdivisions, adjacent series of sections were stained for Nissl and cytochrome oxidase or acetylcholinesterase. Sections were mounted, air dried, dehydrated, and coverslipped.

A separate group of adult rewired ferrets ( $n = 2$ ; Table 1) and all the young postnatal animals used in the present study ( $n = 24$ ; Table 2) received injections of CTB into one eye and of wheat germ agglutinin conjugated to HRP (WGA-HRP) into the other eye. In animals older than P22, intraocular injections of CTB were made as described above, and 2 d later 10  $\mu$ l of 4–5% WGA-HRP (Sigma) in saline was injected into the other eye. Two further days of survival were allowed before perfusion. In animals younger than P22, 2–6  $\mu$ l of each tracer was administered on the same day, and 1–2 days of survival were allowed for transport. The animals were perfused with 2% paraformaldehyde at 4°C for 30 min. The excess fixative was removed from the tissue by subsequent perfusion with 5% and 10% sucrose for 20–30 min (for details, see Angelucci et al., 1996b). Age at perfusion was considered the age of the experiment (Table 2). After cryoprotection, brains older than P14 were sectioned at 40  $\mu$ m in the coronal plane, whereas younger brains were cut at 50  $\mu$ m. One series of sections was post-fixed in 2–4% paraformaldehyde for at least 1 d, soaked for 20 min in 90% methanol and 0.3%  $H_2O_2$  in distilled water to bleach endogenous and injected peroxidase activity, and then processed for CTB immunohistochemistry as described above. The adjacent series was processed using TMB to reveal HRP according to the protocol of Mesulam (1978), lightly counterstained with thionin, and coverslipped.

**Data analysis.** Microscopic analysis of CTB-stained sections was carried out using bright- and darkfield illumination. The WGA-HRP-processed material was analyzed under darkfield and polarized light.

The distribution and termination patterns of the ectopic projections were examined on coronal, parasagittal, and horizontal CTB-stained sections by reconstructing the terminal labeling with a camera lucida, using 10 $\times$  and 25 $\times$  objectives. Axon trajectories were reconstructed at higher magnification (40 $\times$ ) in coronal and horizontal MGN sections. Cytoarchitectonic boundaries and MGN subdivisions in rewired ferrets were identified by matching CTB-stained sections to adjacent sections reacted for Nissl, cytochrome oxidase, and acetylcholinesterase, and by comparison with coronal sections of normal ferret thalami stained with the same methods, as well as with myelin stain. Parcellation of the MGN was also based on the distinct pattern of thalamocortical projections examined in a previous study (Angelucci et al., 1993; Angelucci, 1996).

In adult animals, the size of retino-MGN clusters was estimated in camera lucida reconstructions of CTB terminal labeling by drawing a perimeter around the outermost border of each cluster and measuring cluster diameter in two orthogonal planes. For this analysis, a cluster was defined as an area of tightly packed terminal boutons formed by more than a single axon arbor. Individual, loosely branched axonal arbors were

**Table 2. Intraocular injections in young animals**

|         | Number of animals |    |    |    |     |     |     |     |     |     |
|---------|-------------------|----|----|----|-----|-----|-----|-----|-----|-----|
|         | P4                | P6 | P7 | P8 | P14 | P22 | P25 | P26 | P27 | P29 |
| Rewired | 2                 | 2  | 2  | 2  | 2   | 4   | 1   | 1   | 1   | 4   |
| Normal  | 1                 | 1  |    |    |     | 1   |     |     |     | 1   |

All rewired ferrets were operated on both sides of the brain, with surgery on P1. All animals in the table received an injection of CTB in one eye and WGA-HRP in the opposite eye.

not included in the analysis. Because of the high contrast of CTB staining (see Fig. 1), and the complete filling of fibers and terminal specializations obtained with this tracer (Angelucci et al., 1996b), it was easy to delineate high density terminal zones of clustered boutons. Clusters were then grouped according to the MGN subdivision in which they were located, and for each group, mean values and SEM were calculated separately for the long and the short diameters. No corrections were made for shrinkage because all sections had been treated identically.

To examine how retino-MGN projections are assembled into terminal clusters during development, individual CTB-labeled axonal arbors were reconstructed at various developmental ages (first to fourth postnatal week;  $n = 25$ ) and at adulthood ( $n = 9$ ) using camera lucida and a 63 $\times$  objective. Most axons were drawn within single MGN sections because adjacent series were processed for WGA-HRP (to reveal projections from the opposite eye) or used for various histochemical reactions (to identify MGN subdivisions). Even though it is unlikely that an entire axonal arbor is confined to a 50  $\mu\text{m}$  slice, the exclusion of parts of an arbor should occur randomly across cases, allowing at least qualitative comparisons between populations of axonal arbors at different ages. However, it is likely that the proportion of an axon contained within an MGN section at adulthood is smaller than at early postnatal ages because the MGN grows significantly from P8 to adulthood. For this reason, in the adult cases, some axons were entirely reconstructed in serial MGN sections.

The spatial relationship between inputs from the two eyes in MGN and LP was examined in bilaterally rewired animals that had received an injection of CTB into one eye and of WGA-HRP into the other eye. TMB- and CTB-stained sections were drawn by camera lucida, and adjacent sections were superimposed. To compensate for differential shrinkage caused by the different histological procedures, the magnification of the drawings was adjusted, and adjacent sections were aligned using the lateral edges of the nucleus and vascular landmarks as reference.

*Development of retino-MGN projections and emergence of clusters: quantitative analysis.* The following measurements were performed between P4 and adulthood (Table 2): (1) area of the MGN, (2) area of retinal projections to MGN, (3) percentage of the MGN area innervated by retinal projections, and (4) percentage of retinal projections forming clusters ("clustering index"). A total of 12 cases was used for this analysis (two to three cases per postnatal week and two adult cases). For each case, we selected two representative coronal MGN sections contralateral to the eye injected with CTB, taken at comparable rostrocaudal levels. The caudalmost section was usually located at the border between regions of higher and lower density of projections, whereas the rostralmost section was often in the middle of the high density region. To allow for computerized calculations of optical densities, entire MGN sections were digitized using a CCD camera attached to a microscope and connected to a computer. The density of CTB labeling in MGN was determined by a window smoothing method. For the pseudocolor images shown in Figure 11, *A* and *B*, the color of each pixel corresponds to the density of CTB labeling within a 29  $\mu\text{m} \times 29 \mu\text{m}$  square window centered at that pixel. For each case, the images of MGN sections were normalized so that the brightest red corresponded to median CTB labeling in the LGN of the same case, and the darkest blue to the 85 percentile of the background of the MGN section. Each pixel in the images corresponded to a square of side 4.2  $\mu\text{m}$ .

The area of each MGN section was calculated as the sum of all the pixels in the section. The area of retinal projections to MGN was estimated as the sum of all pixels, with labeling density more than 15.6% of the maximum labeling. Lower density values consisted essentially of the background of the section. Clustered projections were estimated as the percentage of MGN pixels the labeling density of which was more than 46.8% of the maximum labeling. The choice of

this threshold was based on the visual observation that lower density values consisted of sparse, nonclustered retino-MGN fibers. A smoothing and thresholding procedure was implemented to eliminate isolated pixels with high density values. The procedure effectively eliminated clusters composed of a small number of pixels. The clustering index was defined as the percentage of the retinal projection area occupied by clustered projections. It is important to point out that the values obtained (reported in Fig. 11*C–F*) are relative measures and do not reflect actual values. Moreover, the clustering index underestimates the percentage of retinal projections forming clusters, especially at later postnatal ages, because a cluster in our analysis consists only of the densest core (represented in orange-red in Fig. 11*A,B*) of an actual retinal cluster in MGN.

## RESULTS

### Methodological considerations

Redirection of retinal inputs to inappropriate thalamic nuclei has been shown previously to occur when some of the normal retinal targets (SC and/or LGN) are ablated, and alternative space is created by partially deafferenting an ectopic target (Schneider, 1973; Kalil and Schneider, 1975; Frost, 1981, 1982, 1986; Sur et al., 1988; Roe et al., 1993). In these earlier studies, however, the MGN was only partially deafferented because only the brachium of the inferior colliculus was sectioned. In the course of a series of studies on thalamic specification, we reassessed the lesion paradigm previously used in this laboratory. We found that extensive deafferentation of the MGN, including both brachial and extra-brachial ascending pathways (see Materials and Methods), combined with partial or complete ablation of SC, was sufficient to induce maximal retinal innervation of the auditory thalamus. Ablation of the LGN was neither sufficient nor necessary. Moreover, rerouting of retinal fibers to the MGN was obtained consistently with this new type of manipulation, likely because of a more comprehensive deafferentation of the nucleus (Angelucci, 1996).

The observations described in the present paper were made in animals that were rewired 1 d after birth according to the new lesion paradigm. Whereas the MGN was extensively deafferented, the visual cortex and the LGN were completely spared. However, the SC was extensively cauterized because deafferentation of the auditory thalamus requires removal of contralateral inputs that reach the MGN via the commissure of the SC, and of the deep layers of SC that project to the ipsilateral MGN (in cat: Graham, 1977; Calford and Aitkin, 1983; Morest and Winer, 1986; in ferret: Angelucci, 1996). As a result of these lesions, retinal afferents invaded the MGN as well as another ectopic thalamic target, the lateral posterior nucleus (LP). The SC is a source of inputs to LP (in cat: Graybiel, 1972; McIlwain, 1978; Graybiel and Berson, 1980; Kawamura et al., 1980; Caldwell and Mize, 1981; Benedek et al., 1983; in ferret: Angelucci, 1996); thus, ablation of SC results in partial deafferentation of LP. Indeed, we observed that the extent of novel retinal projections to LP directly correlated with the extent of the superior collicular lesion, i.e., with the extent of LP deafferentation.

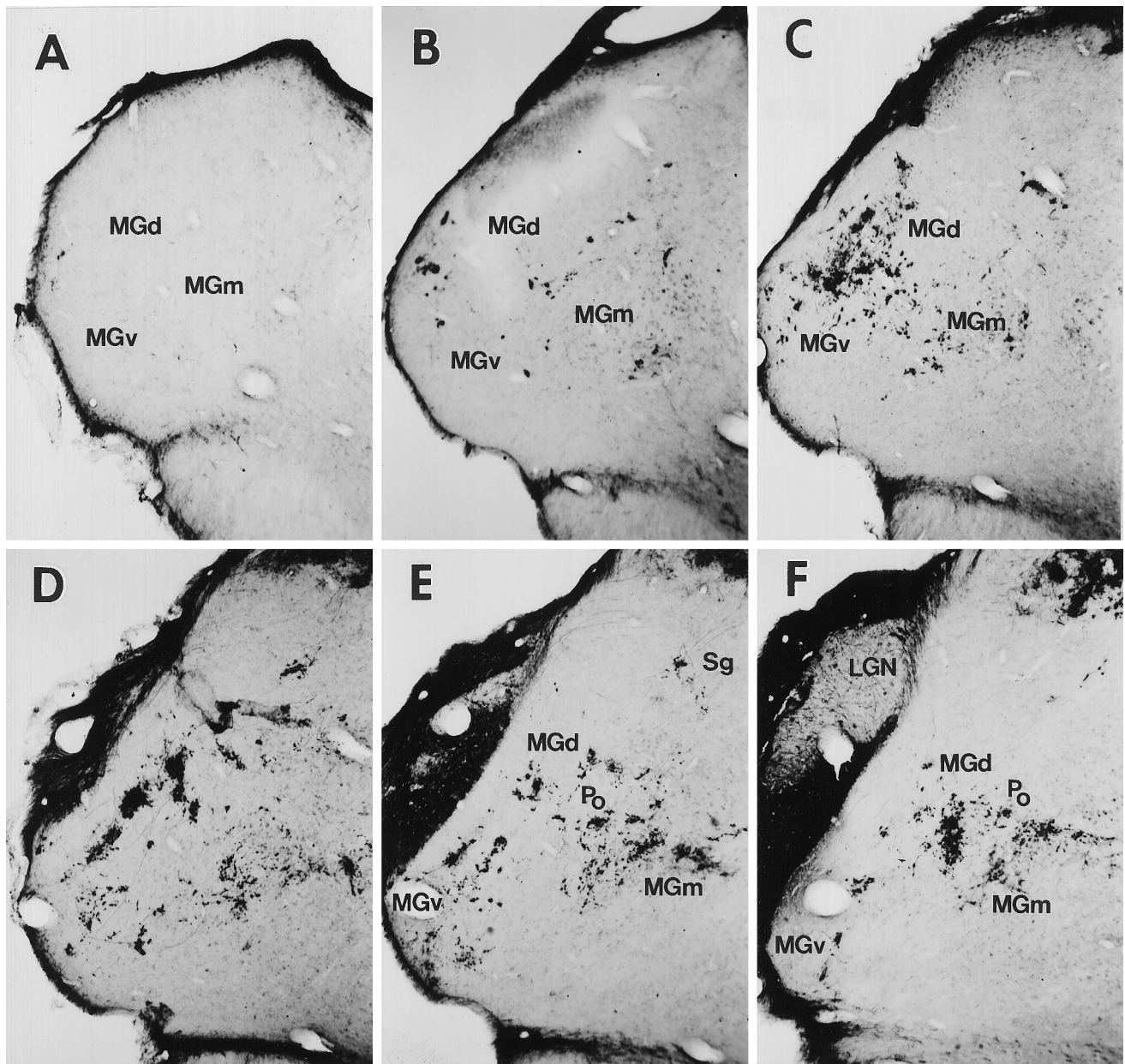


**Figure 1.** Distribution and pattern of termination of retinal projections to the MGN in an adult rewired ferret. Retino-MGN projections were labeled by injecting CTB into the contralateral eye (case F94–97; Table 1). *A–F*, Caudal-to-rostral sequence of coronal sections through the MGN. The spacing between sections is indicated in Figure 2. Note that retinal fibers form terminal clusters scattered throughout the MGN subdivisions (*MGv*, *MGd*, *MGm*), predominantly in the rostral half of the nucleus. Patches in *MGv* are oriented and aligned along an oblique dorsoventral axis (see Results). MGN subdivisions for *D* are indicated in Figure 3*A*. The injection also labels projections from the contralateral eye to the LGN, marked in *F*. The LGN region free of label corresponds to the projection zone from the ipsilateral, noninjected eye. Dorsal is *up*; medial is to the *right*. Scale bar, 500  $\mu$ m.

An additional advantage of the new surgical manipulation was that it produced virtually no distortion in the shape, size, and relative position of the various thalamic nuclei. Thus, the cytoarchitectonic subdivisions of the thalamus and of the MGN could be easily identified in Nissl stained sections, allowing comparisons across experimental and normal cases. Our parcellation of the normal ferret MGN into various subdivisions was based on matching different staining methods such as Nissl, myelin stain, cytochrome oxidase, and acetylcholinesterase, and on the distinct pattern of MGN projections to the auditory cortex (Angelucci et al., 1993; Angelucci, 1996). Following Morest (1964) and others

(Imig and Morel, 1988; Winer, 1992), we could distinguish four main nuclei in the MGN of the ferret: the dorsal (*MGd*), ventral (*MGv*), and medial (*MGm*) divisions, and the lateral nucleus of the posterior thalamic complex (*Po*) (Fig. 1). We did not attempt to further subdivide *MGv* and *MGd* into subsidiary nuclei because our material did not allow for a clear demarcation of such regions. However, within the dorsal division we could distinguish the suprageniculate nucleus (*Sg*) from the rest of *MGd* because of the larger size and lower density of its cell bodies. *Sg* constitutes the medial part of the dorsal division, bordered ventrally by *MGm* and dorsally by the LP/Pulvinar nucleus.

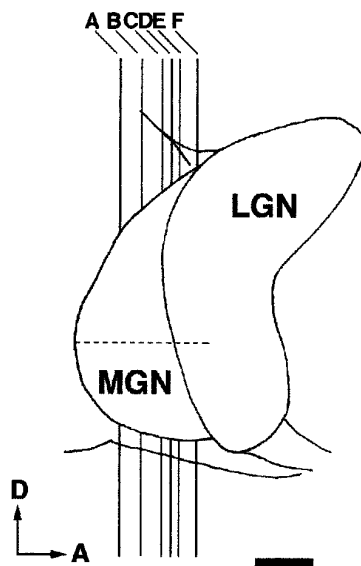


**Figure 2.** Lateral view of the dorsal thalamus. The vertical lines (A–F) indicate the approximate anteroposterior level of each MGN section shown in Figure 1. The horizontal dashed line marks the rostrocaudal extent of the MGN. D, Dorsal; A, anterior. Scale bar, 1 mm.

### Retinal projections to novel thalamic targets in adult animals

After intraocular injections of CTB in adult rewired animals, retinal fibers were observed in all the normal targets, as well as in two ectopic targets, MGN and LP. A few retinal axon arbors, usually arising from the LP or pretectum, could occasionally be detected also in the ventroposterior lateral thalamic nucleus (data not shown). The overall pattern of CTB labeling in normal retinal targets seemed indistinguishable from that described in normal animals (Angelucci et al., 1996b) and included the dorsal and ventral LGN, the lateral part of the pulvinar, remnants of the upper strata of the SC (when not completely ablated), the pretectal nuclei (PT), the accessory optic nuclei, and the hypothalamus. Because the LGN was not lesioned in the animals used in the present study, retino-LGN projections in rewired ferrets seemed organized in eye-specific layers and on and off sublayers, as described previously for normal retino-LGN afferents (Hahm et al., 1991). Myelinated fiber tracts such as the optic and the accessory optic tracts were also clearly labeled by CTB.

#### Projections to the medial geniculate nucleus

In rewired ferrets, a significant number of retinal axons were found to arborize in the medial geniculate nucleus (Fig. 1). The areal extent of contralateral retinal projections within MGN and the percentage of the MGN area innervated by retinal inputs were quantified (see below).

We then examined the distribution and termination patterns of retinal inputs within the auditory thalamus. Retinal axons were found to innervate all the subdivisions of the MGN: MGv, MGd, MGm, and Po (Fig. 1). However, terminal arbors were most abundant in the anterior half of the nucleus and in MGv, whereas few axons terminated in the caudal third of MGN (Figs. 1–3). This rostral bias is apparent in Figure 1, which shows a caudorostral sequence of coronal sections through the MGN contralateral to the CTB-injected eye, and in Figure 3*B* illustrating contralateral retino-MGN projections in the horizontal plane.

Retinal projection patterns in MGN were fairly stereotyped

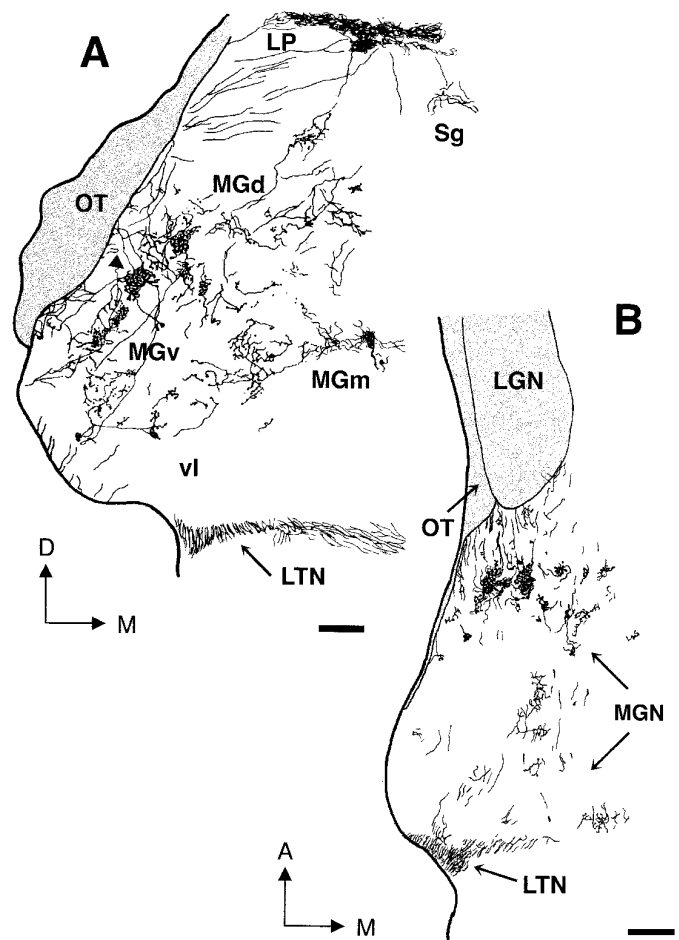


**Figure 3.** Trajectories of retinal axons that innervate the MGN in adult rewired animals. *A*, Camera lucida drawing of the coronal MGN section illustrated in Figure 1*D*, shown at higher magnification to demonstrate axon trajectories. Note that retinal axons enter the MGN from all around the nucleus. Terminal clusters of retinal projections are more evident in MGv and MGd. One cluster (arrowhead) is partly reconstructed at higher magnification in Figure 4*B*. *B*, Camera lucida drawing of a horizontal MGN section showing axon trajectories in the anteroposterior dimension. Clusters of retinal projections are elongated anteroposteriorly. LTN, Lateral terminal nucleus; OT, optic tract; vl, ventrolateral nucleus of MGv; A, anterior; D, dorsal; M, medial. Scale bars, 200  $\mu$ m.

across different animals. Typically, retinal projection zones were organized into clusters of terminals scattered throughout the nucleus (Figs. 1, 3), but overall they innervated only part of the MGN (Fig. 1). Clusters in MGv and Po, and in the lateral parts of MGd, seemed more dense and more restricted than those in MGm and in the medial aspect of MGd (Sg). In MGm, retinal projections had generally more diffuse terminal arborizations. In the coronal plane, clusters in MGv seemed elongated, with the longer axis oriented in the dorsoventral dimension (Figs. 1, 3*A*), whereas in horizontal sections they were elongated rostrocaudally (Fig. 3*B*). Furthermore, in coronal sections of MGv, individual patches often seemed to align along a dorsoventral axis (Figs. 1*C–E*, 3*A*; see also Fig. 6). In contrast, orientation and alignment of clusters were not typically observed in MGm or MGd (Figs. 1*C–F*, 3*A*; see also Fig. 6). The above observations were quantified by measuring cluster size. In coronal MGv sections, the long (dorsoventral) axis of a patch had a mean length of 138  $\mu$ m (SEM = 9.33;  $n$  = 13), and the shorter axis (mediolateral) of 80

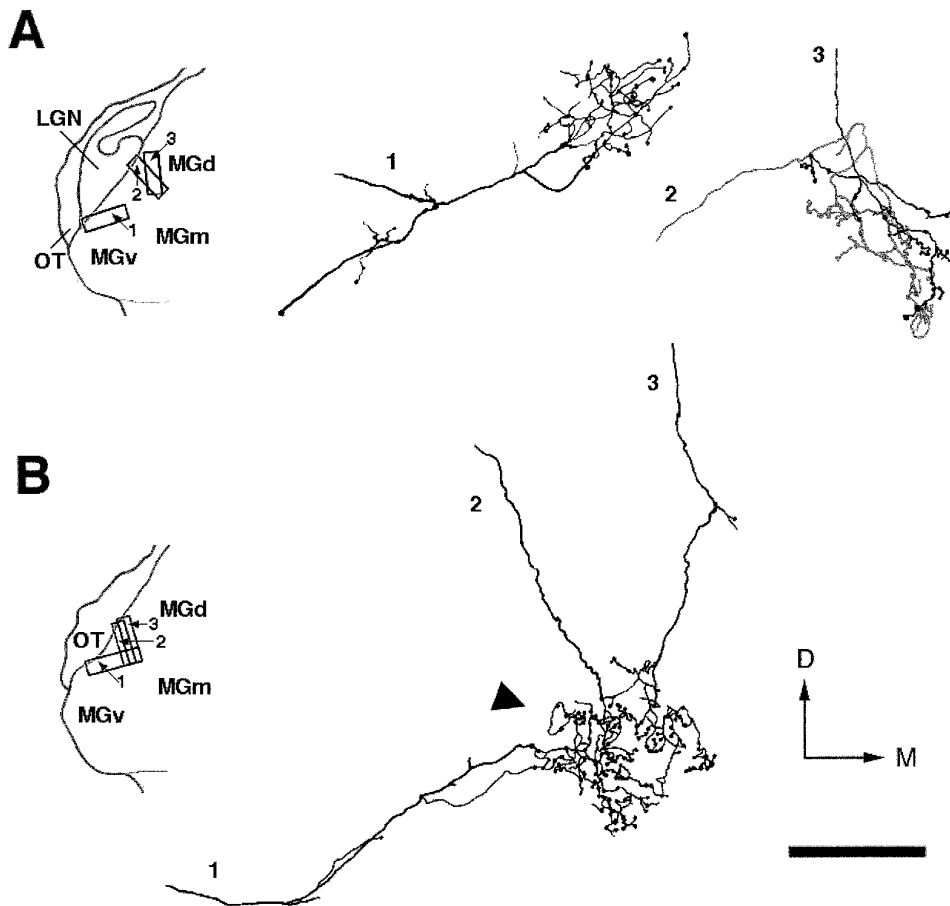


**Figure 4.** Camera lucida reconstructions of six retino-MGN axonal arbors in adult rewired ferrets. These axons have focal terminal arbors with large clustered boutons (see Results). The insets on the left show a coronal view of the location of each reconstructed axon within MGN. *A*, Axons 2 and 3 are shown in gray and black, respectively, to demonstrate the overlap between their terminal arbors. *B*, Partial reconstruction of one cluster (arrowhead) shown in Figure 3*A*. This cluster was formed by the terminal arbors of several axons (see Fig. 3*A*). Here we reconstructed only three of them. *OT*, *D*, and *M* are as in Figure 3. Scale bar, 100  $\mu$ m.

$\mu$ m (SEM = 7.4;  $n$  = 13). In the horizontal plane, mean patch sizes in MGv were 61  $\mu$ m (SEM = 5.18;  $n$  = 13) along the mediolateral axis, and 151  $\mu$ m (SEM = 13.59;  $n$  = 13) along the rostrocaudal axis. The dorsoventral and rostrocaudal axes of the clusters were significantly longer than the mediolateral axis ( $p$  < 0.001 in both cases, Student's  $t$  test), indicating that clusters in MGv are elongated both dorsoventrally and rostrocaudally. Cluster size was not significantly different in the horizontal and coronal planes ( $p$  > 0.05). In MGd, clusters had mean sizes of 57  $\times$  158  $\mu$ m in the coronal plane (SEM = 5.67,  $n$  = 7 for the short axis; SEM = 11.78,  $n$  = 7 for the long axis), indicating that clusters in MGd are also elongated. However, the longer axis of the patches in this division did not bear any consistent relation to any particular dimension, i.e., clusters were not oriented. Because clusters in MGm were less restricted than in other MGN subdivisions, it was more difficult to measure patch sizes in this division. Our measurements indicated that clusters vary considerably in size and shape in MGm (mean size in the coronal plane: 68  $\times$  174  $\mu$ m; SEM = 5.5,  $n$  = 7 for the short axis; SEM = 20.3,  $n$  = 7 for the long axis). Clusters in MGm, like those in MGd, were not oriented.

Axon trajectories were examined in coronal and horizontal MGN sections (Fig. 3). Retinal axons entered the MGN after several distinct pathways that generally correlated with their final destination within the nucleus. In the coronal plane, some axons entered laterally and dorsolaterally, arising directly from the optic tract in more caudal sections, and entering through the LGN at more rostral levels. These axons tended to arborize soon after entering the nucleus and generally terminated within a cluster in

MGv or in the lateral aspects of MGd (Fig. 3*A*). They seemed to have restricted terminal branched arbors with large clustered boutons. Another group of axons could be detected in coronal sections, entering the MGN dorsomedially through the LP or pretectum and terminating in MGd (including Sg), Mgm, and Po (Fig. 3*A*). Some of these axons coursed for more than 1 mm within MGN without arbors, branches, or boutons *en passant* before terminating. In the coronal plane, a third group of retinal axons entered the MGN ventrally, through the lateral terminal nucleus and ventral accessory optic tract, and usually terminated in MGm. The axons that innervated the medial division seemed to have sparser and less focal terminal arborizations, with boutons often arranged in strings. Observation of axonal trajectories in the horizontal plane indicated that retinal axons entered the MGN also rostrally, through the optic tract and LGN, as well as caudally from nuclei of the accessory optic system (Fig. 3*B*). Indeed, when compared with the observations made in coronal sections, it was clear that the majority of retinal axons originated from the optic tract and LGN, followed a rostrocaudal trajectory, and terminated predominantly in the anterior portion of MGN (compare Fig. 3*A* and 3*B*).

To understand the precise anatomical organization of retinal terminal clusters, we reconstructed individual representative CTB-stained axonal arbors. Because our aim was to examine how individual axon arbors contribute to the formation of clusters, we preferentially selected for reconstruction axons that terminated within clusters. Moreover, because clusters were better defined in MGv and MGd, we reconstructed axonal arbors only in these subdivisions (Fig. 4). These arbors had simple terminations with a single,

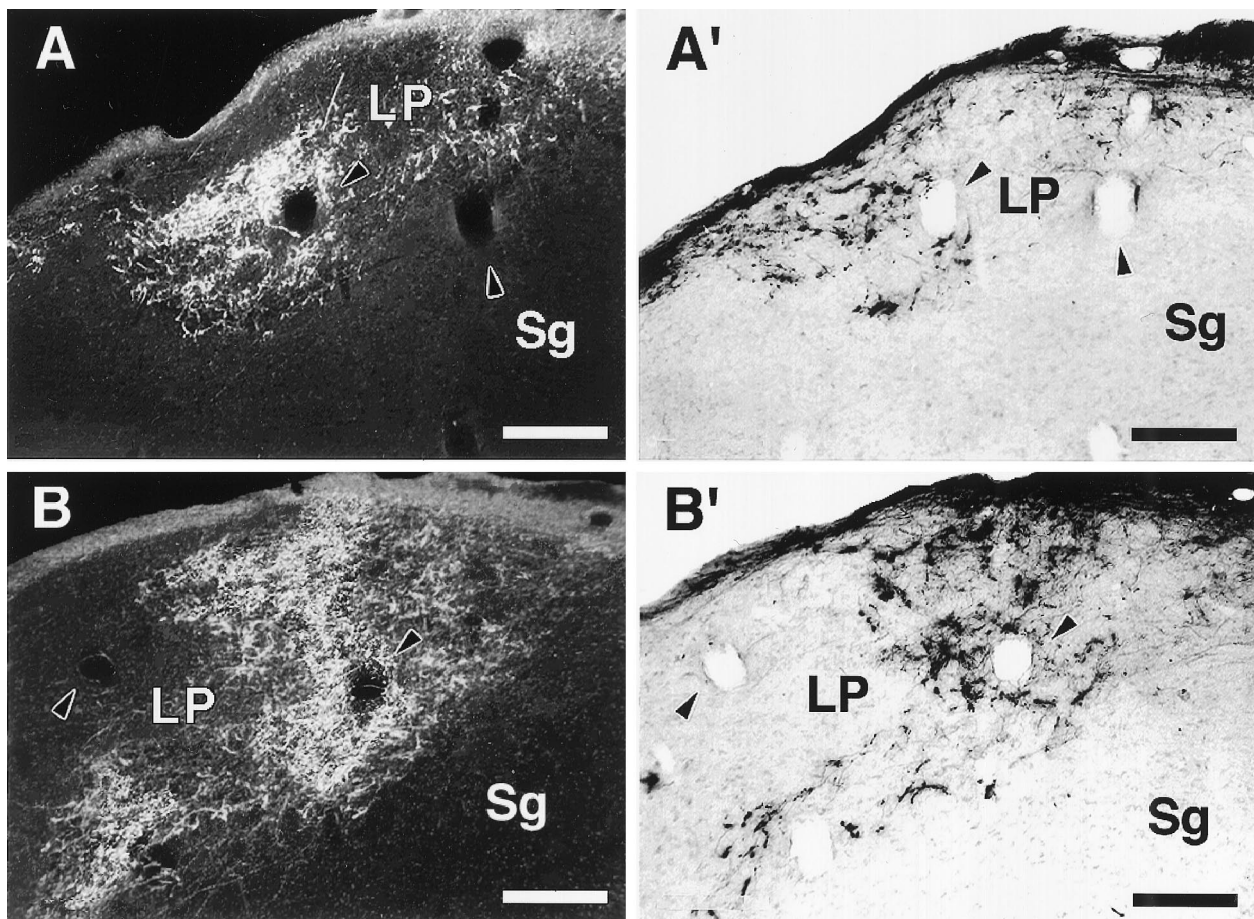


**Figure 5.** Retinal inputs to the LP in an adult rewired ferret. *A, B*, Dark-field micrographs of retino-LP projections labeled by an injection of WGA-HRP in the contralateral eye. *A', B'*, Bright-field micrographs of ipsilateral retino-LP projections labeled with CTB. Sections in *A* and *B* are immediately adjacent to sections in *A'* and *B'*, respectively. *Arrowheads* point to corresponding blood vessels in adjacent sections. A composite drawing of *A* and *A'* is shown in Figure 7. Note the terminal slab-like pattern of retinal projections to LP. Dorsal is *up*; medial is to the *right*. Scale bars, 200  $\mu$ m.

well defined focus, had large clustered boutons, and closely resembled in morphology a group of retino-MGN axon arbors described previously by Pallas et al. (1994; see their Figs. 6 and 7). Clusters were not formed by individual axon arbors but by the convergence and overlap of several arbors. This is clearly indicated in Figure 4*B*, which shows an example of three different axons entering the MGN at three separate points along the optic tract, converging onto the same region and forming overlapped terminal arbors. Axon arbors were mostly restricted to a single cluster and did not send branches to several clusters. A previous study (Pallas et al., 1994), in which retino-MGN axons were reconstructed in the parasagittal plane, similarly showed that the majority of these axons form only one focal terminal arbor in MGN.

Because of the large number of labeled axons in the optic tract, as well as in all the normal retinal targets that surround the MGN, it was not possible to follow axons for any distance outside the auditory thalamus. Thus, whereas we occasionally observed fibers in the optic tract, LGN, LP, and accessory optic nuclei sending a branch into the MGN, it is not clear whether retino-MGN axons are collaterals of fibers projecting to other targets. For the same reason, we cannot rule out the possibility that an individual axon sends multiple collaterals to the MGN that enter this nucleus at several loci along the course of the axon.

#### *Projections to the lateral posterior nucleus*

In rewired ferrets, the LP received a substantial direct input from the retina (Fig. 5). Here, the retinal projection zones were consistently more extensive than in the MGN. As in rewired MGN and normal LGN, projections from the contralateral eye within LP were significantly more numerous than those from the ipsilateral eye (Fig. 5).

Retinal projections were most dense in the caudal half of LP. Posteriorly, they occupied the caudalmost part of the nucleus, which at this level forms a dorsomedial rim that caps the MGN (Fig. 5*A,A'*); more anteriorly they were located in the medial portion of LP (Fig. 5*B,B'*). In contrast to the patchy pattern of termination observed in the auditory thalamus, retinal axons in LP tended to form terminal slabs that sloped from dorsomedial to ventrolateral (Fig. 5). The location and shape of these retinal termination zones bear striking resemblance to the terminal zones of superior collicular inputs to the pars medialis of LP (LPm) described previously in cats by Graybiel and Berson (1980). It is not surprising that in rewired ferrets retinal projections would terminate predominantly in LPm because, as a result of SC ablation, this should be the most extensively deafferented LP subdivision in our preparation (see above).

Retinal axons that innervate LP followed two main pathways.

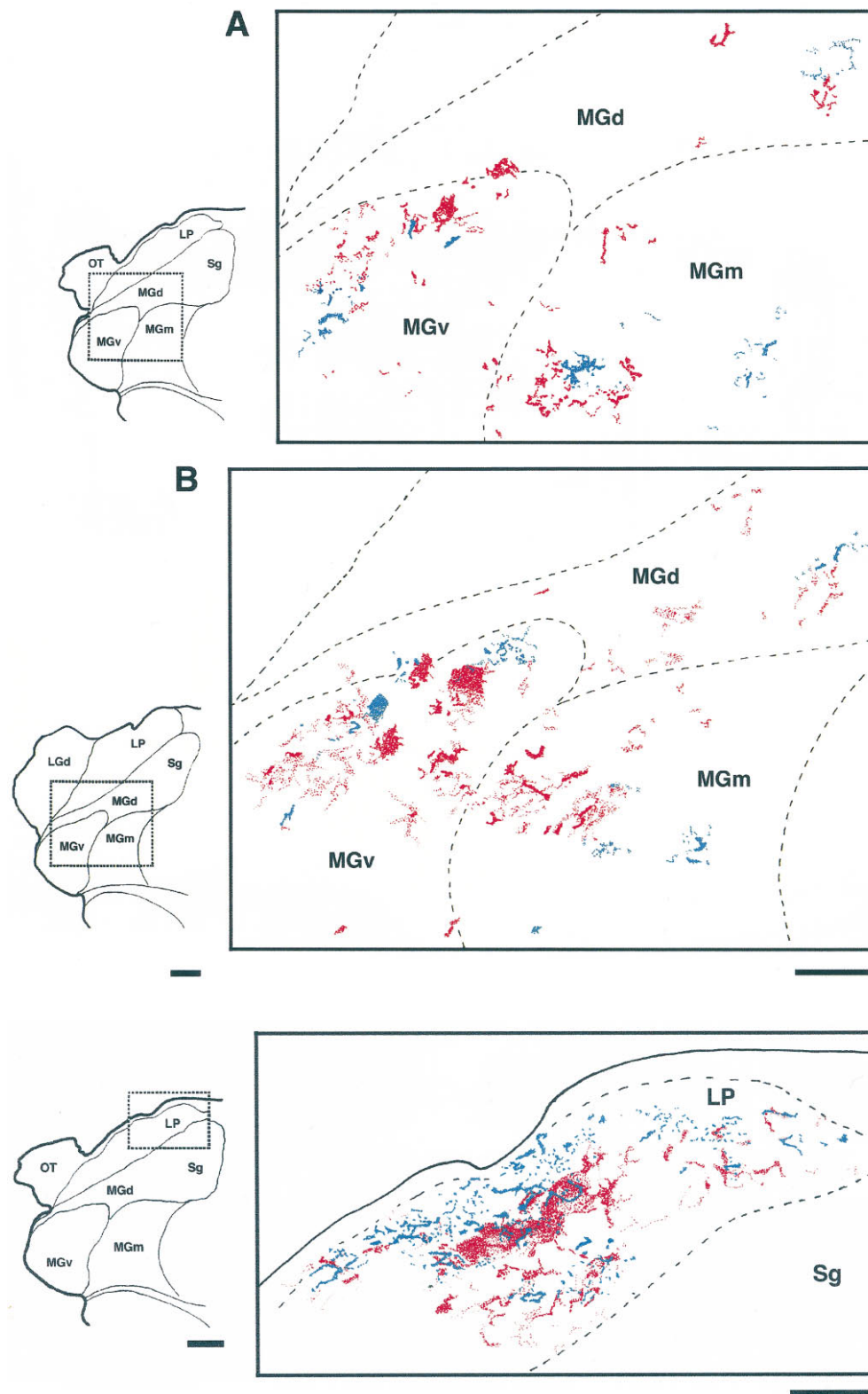


**Figure 6.** Spatial relationship between eye-specific inputs in the MGN of adult rewired ferrets. *A, B (right)*, Composite reconstructions of the retinal label from each eye, obtained by superimposing camera lucida drawings of two adjacent MGN sections (see Materials and Methods). Projections from the contralateral eye, stained with WGA-HRP, are represented in *red*, whereas CTB-stained ipsilateral projections are represented in *blue*. Only terminal zones are plotted (fibers are not shown). Note that retinal inputs from the two eyes terminate mainly in the same regions of MGN in a nonoverlapping manner (see Results). Right scale bar, 200  $\mu\text{m}$  (valid for both *A* and *B*). *A, B, Left*, Camera lucida drawings of coronal thalamic hemisections, showing the location (*insets*) of the retinal label drawn at higher magnification on the *right*. Left scale bar, 500  $\mu\text{m}$  (valid for both *A* and *B*). Abbreviations as in previous figures. Dorsal is *up*; medial is to the *right*.

**Figure 7.** Eye-specific segregation in the lateral posterior nucleus. *Right*, Composite camera lucida drawing of retino-LP projections arising from each eye, obtained by superimposing section *A* and *A'* of Figure 5 (see Materials and Methods). Contralateral retinal projections are represented in *red*. Projections from the ipsilateral eye are represented in *blue*. Only terminal zones are illustrated. Projections from the two eyes form parallel, largely segregated slabs in LP (see Results). Right scale bar, 200  $\mu\text{m}$ . *Left*, same as Figure 6 (*left*). Left scale bar, 500  $\mu\text{m}$ . Abbreviations as in previous figures. Dorsal is *up*; medial is to the *right*.

A first group of axons entered the nucleus laterally and dorso-laterally, arising directly from the optic tract. Optic tract fibers in normal adult ferrets cross the LP/Pulvinar on their way to the SC and PT, but do not normally terminate in LP. A second group of retinal fibers reached LP dorsomedially through the pretectum.

**Binocular organization**

Both eyes projected to the same regions within MGN and LP. In MGN, clusters of terminals related to one eye were often adjacent to, but spatially segregated from, clusters related to the other eye (Fig. 6). However, because clusters from the contralateral retina were

more numerous, it was not uncommon to detect contralateral clusters not apposed to ipsilateral ones. Isolated clusters of ipsilateral axons were less commonly observed. It is unlikely that the spatial proximity of terminals from the two eyes represents the outcome of a random phenomenon, given that retinal fibers innervate specific focal portions of the available terminal space in MGN.

Spatial segregation according to the eye of origin was observed also in the lateral posterior nucleus. In caudal LP, eye-specific segregation was more evident and occurred in the form of parallel, largely nonoverlapping “slabs” oriented from dorsomedial to ventrolateral, in coronal sections (Fig. 7). However, in more rostral sections it was not uncommon to observe areas of partial overlap between projections from the two eyes. This overlap might have been related to the plane of sectioning. In fact, at more rostral levels, LP expands and its ventromedial border gradually slopes dorsally so that the overall orientation of the nucleus progressively changes, moving rostralwards. Accordingly, the slabs of retinal terminals seemed more vertically oriented in rostral (Fig. 5*B,B'*) than in caudal LP (Fig. 5*A,A'*). Thus, it is possible that at more rostral LP levels, eye segregation would be better observed in other planes of section.

#### Development of retinal projections to the medial geniculate nucleus

The anatomical organization of the mature ectopic retinothalamic projections into terminal clusters and eye-specific domains was reminiscent of clustering and eye-specific segregation of retinal afferents within some normal targets, such as the LGN and SC. By analogy with clustering in LGN and SC, the mature patterns of ectopic retinothalamic connections may result from the refinement of initially diffuse and largely overlapped projections. Alternatively, such patterns may be established by the initial ingrowth and arborization of retinal axons into specific regions of the ectopic targets. To differentiate between these two possibilities, we examined the development of retinal termination patterns in the MGN.

At birth in ferrets, the auditory thalamus was well differentiated and distinguishable from adjacent thalamic nuclei in Nissl-stained sections. However, its cytoarchitectonic pattern seemed fairly homogeneous, and nuclear subdivisions were hard to assess based only on Nissl staining. Thus, in early postnatal animals we did not attempt to subdivide the MGN.

#### Qualitative observations

We first investigated whether the retino-MGN projection present in adult rewired ferrets is created *de novo*, or by the stabilization of transient retinal projections to this nucleus. To this end, normal ferret kits received intraocular injections of CTB (Table 2). In normal ferrets, retinal axons did not terminate in MGN at any age (data not shown). However, at all ages examined, some optic tract axons directed toward more distal targets crossed the dorsolateral aspect of MGN at rostral levels, often forming fascicles. These axons were few in number at P4–P6 and, as the MGN increased in size, were displaced progressively more dorsolaterally so that by P27 only a few of them traversed the nucleus very superficially. However, none of these axons branched in the auditory thalamus. In contrast, in rewired ferrets at P4 and P6, the MGN was invaded by a large number of simple, fairly unbranched retinal axons that terminated in this nucleus. Thus, retinal projections to MGN are created *de novo* in rewired ferrets.

We then examined the development of retino-MGN projections both at the population (Fig. 8) and at the single axon arbor (Fig.

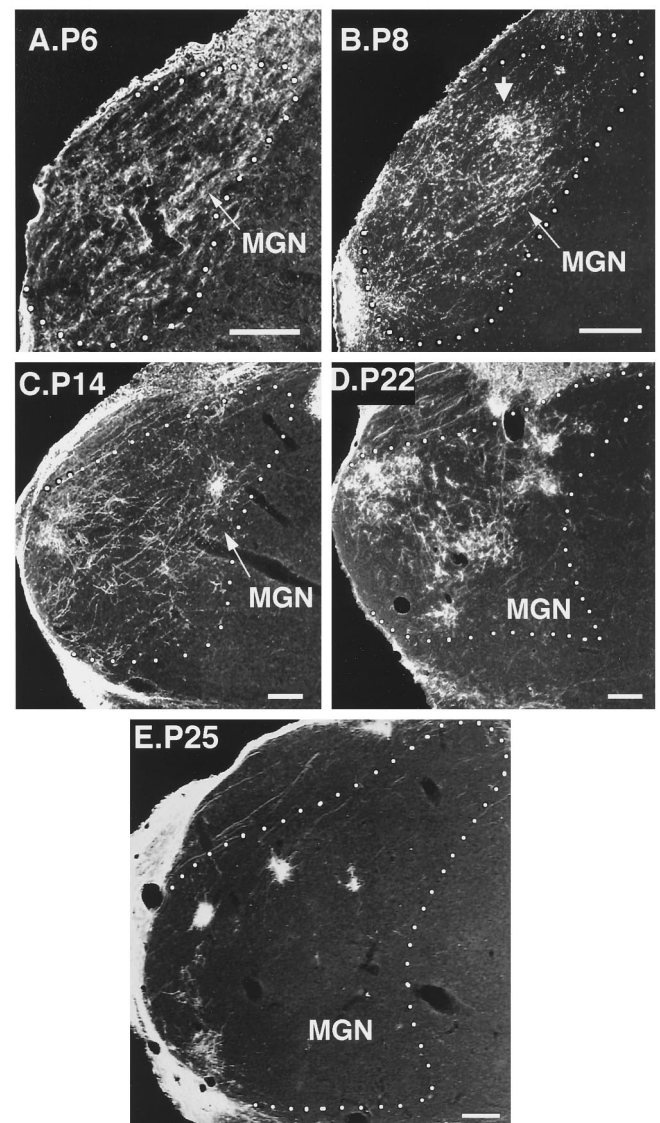


**Figure 8.** Emergence of clustered retinal projections to the MGN in young postnatal rewired ferrets. *A–E*, Developmental sequence of coronal MGN sections. Retino-MGN projections were labeled by injecting CTB in the contralateral eye at various developmental ages. Postnatal (*P*) ages are indicated at the side of each figure. White dotted lines outline the contour of the MGN. Note that clustering of retino-MGN projections occurs progressively over development. Arrow in *B*, A tendency to cluster first appears at P8. Dorsal is up; medial is to the right. Scale bars, 200  $\mu$ m.

9) level. At P4, both contralateral and ipsilateral retinal projections had already invaded the MGN. During the first week of development, the retino-MGN projection seemed diffuse (Fig. 8*A*), and occupied most of the mediolateral and anteroposterior extent of the nucleus. Retinal fibers entered the MGN from all around, as described above for the adult projection. Representative individual axons at P4 and P6 had at most a few short branches, traversed the nucleus for long distances in all directions, and had bouton-like enlargements along their course. Axons with these characteristics constituted the majority of the projection up to P8, and many were still present at the end of the second postnatal week (Fig. 9, axons 1 and 2).

During the second postnatal week, the projection was still very diffuse, although a tendency to cluster appeared around P8 in

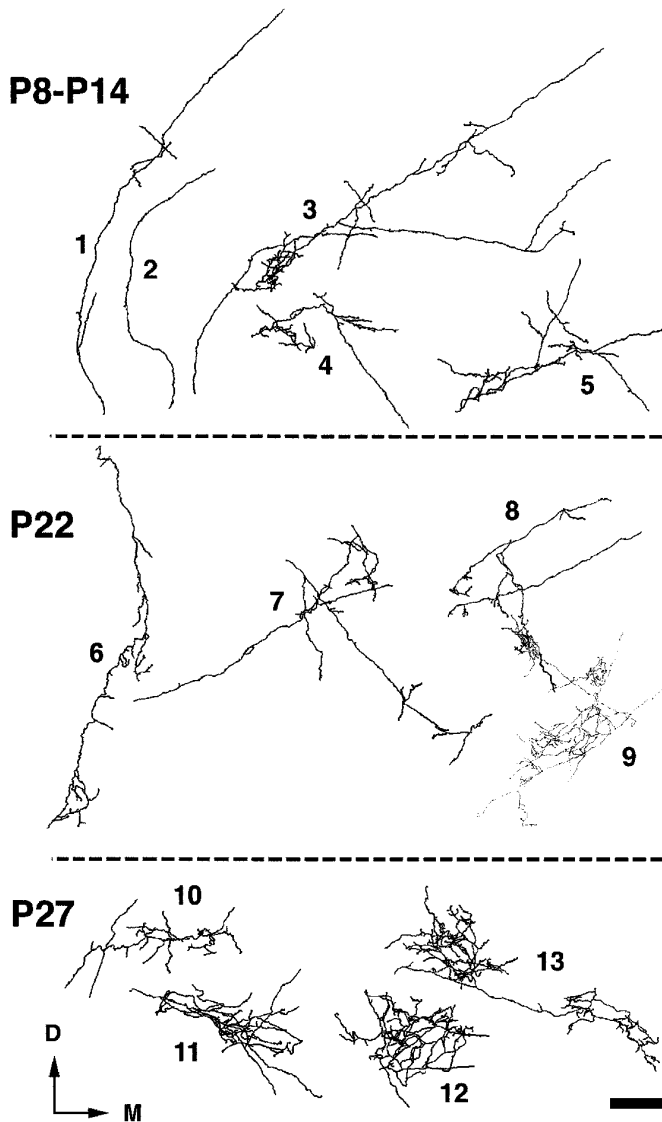


**Figure 9.** Camera lucida reconstructions of 13 retino-MGN axonal arbors during the second and fourth postnatal weeks of development. Postnatal ages (*P*) are indicated on the left of each panel. All axons shown were reconstructed within single MGN sections. Axons 1 and 2 have few (1) or no (2) branches and run for long distances in MGN, resembling 1- and 2-week-old axons (see Results). Axons 3–7 have begun to form arbors and send long branches to distant regions in MGN. Axons 8 and 9 are restricted to one MGN subdivision and send branches to several clusters. These axons are shown in black (8) and gray (9) to demonstrate the overlap of one of their terminal arbors. Axons 10–13 have more elaborate arbors restricted to a single cluster. *D*, Dorsal; *M*, medial. Scale bar, 100  $\mu$ m.

some areas (Fig. 8*B*, arrow), and by P14 clusters were even more apparent (Fig. 8*C*). Many axons were still very simple, resembling 1-week-old axons (see above), but by the end of the second postnatal week many had begun to form arbors (Fig. 9, axons 3–5). These arbors were very extensive, often sending branches to all the subdivisions of the MGN, which by this age had become discernible in Nissl-stained sections. Figure 9 shows an example of such an axon (axon 3) forming an arbor in MGv that contributed to the formation of a cluster. From this arbor, two long collaterals departed at an acute angle, with one collateral terminating in Sg and the other in MGm.

By the end of the third postnatal week, most of the projection had become clustered, but axonal branches running between clusters were still evident in some animals (Fig. 8*D*). During the following week, clusters became denser and further restricted, and the overall pattern of retino-MGN projections seemed nearly adult-like (Fig. 8*E*). Moreover, the characteristic orientation and alignment of clusters along a dorsoventral axis in MGv was evident at P27 (Fig. 8*E*; see also Fig. 10*D*) but not yet at P22 (Fig. 8*D*; see also Fig. 10*C*). Figure 9 shows some examples of reconstructed axon arbors from the fourth postnatal week. At P22, some axons had fairly simple arbors and still coursed for very long distances within the MGN gray matter emitting simple branches all along their length (Fig. 9, axons 6 and 7). Axons of this type were not observed at or after P25. Other axons had more complex arbors that, although confined to one MGN subdivision, were still fairly large and sent branches to more than one cluster (Fig. 9, axons 8 and 9). At P27, most arbors were more elaborate and much more focal than at previous ages (Fig. 9, axons 10–13) and were mostly confined to individual clusters. Comparisons of 4-week-old arbors (Fig. 9) with adult arbors (Fig. 4, this study, and Figs. 6 and 7, Pallas et al., 1994) indicate that, even though the overall pattern of retino-MGN projections seemed adult-like by P22–P27 (compare Figs. 8*D,E* and 10*C,D* with Figs. 1 and 6, respectively), minor refinements of individual axon arbors were still taking place after P27.

The emergence of eye-specific segregation was studied by superimposing CTB stained sections on adjacent sections processed for WGA-HRP (Fig. 10). During the first postnatal week of development, afferents from the two eyes were largely diffuse and terminated over the same MGN regions in an overlapped manner (Fig. 10*A*). At P14, even though clustering had already begun, overlap between inputs from the two retinæ was still evident (Fig. 10*B*). Over the next 2 postnatal weeks, projections from the two eyes progressively segregated into eye-specific regions within the MGN, with clear eye-specific domains evident between P22 and P27 (Figs. 10*C,D*). Segregation of contra- and ipsilateral inputs in LP was also fully established by the end of the fourth postnatal week (Fig. 10*D*).

#### Quantitative observations

All measurements were performed on digitized and normalized CTB-stained MGN sections (Fig. 11*A,B*; see Materials and Methods).

The MGN (including all its subdivisions) increased in mean area by 4.8-fold from P4 to P22 ( $p < 0.001$ , Student's *t* test), and by 50% between P22 and adulthood ( $p < 0.001$ ). Overall, there was a 7.7-fold increase in mean MGN area from P4 to adulthood ( $p < 0.001$ ; Fig. 11*C*). The mean area of the retino-MGN termination zones peaked at P22, with a 4.3-fold increase in extent from the first to the end of the third postnatal week ( $p = 0.025$ ). The mean area of retinal projections at the end of the fourth week of development was not significantly different from the mean retinal projection area at the end of the third postnatal week ( $p = 0.2$ ). Between P27 and adulthood, no significant changes in the extent of retino-MGN projections were observed ( $p = 0.2$ ). Overall, the retinal projection area increased by  $\sim 3.5$ -fold between P4 and adulthood ( $p < 0.001$ ).

From the above results, it follows that early in development retinal projections occupy a much larger proportion of MGN than at adulthood. Between the first and the third postnatal weeks, the percentage of MGN innervated by retinal fibers remained essentially unaltered ( $p = 0.7$ ; Fig. 11*E*) because

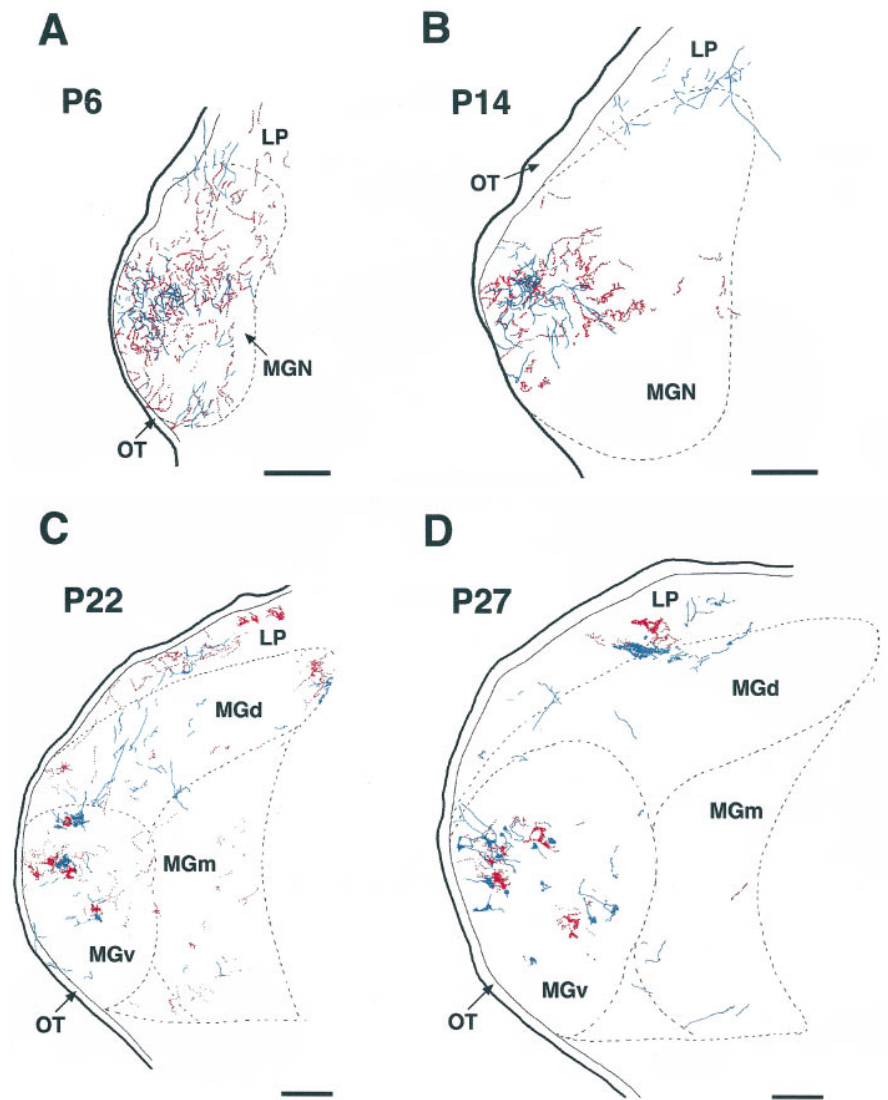


**Figure 10.** Emergence of eye-specific segregation in the MGN. *A–D*, Composite camera lucida drawings of the retinal label from each eye at four different ages. Postnatal (*P*) ages are indicated in each panel. Projections from the contralateral eye are shown in *red* and were labeled with WGA-HRP; CTB-labeled ipsilateral projections are shown in *blue*. Projections from the two eyes are initially overlapped (*A*) but progressively segregate into eye-specific domains (*B–D*). Abbreviations as in previous figures. Dorsal is *up*; medial is to the *right*. Scale bars, 200  $\mu\text{m}$ .

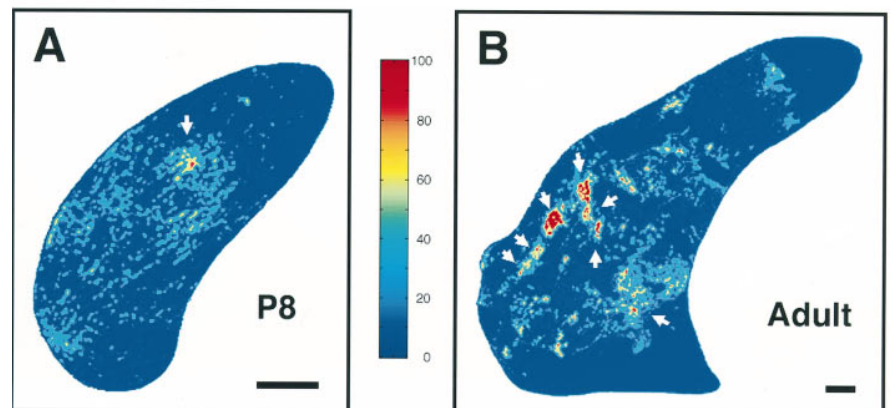


**Figure 11.** Summary of the developmental changes occurring in the MGN and the retino-MGN projections in reared ferrets. *A, B*, Pseudocolored representations of normalized optical densities of CTB-labeled retinal projections to the MGN at P8 (*A*) and adulthood (*B*). The brightest *red*, denoted as 100% in the color key, represents the densest staining and corresponds to median CTB labeling in the LGN (see Materials and Methods). *A* and *B* are computer-generated images of the same MGN coronal sections shown in Figures 8*B* and 1*D*, respectively. *Arrow* in *A* points to the same cluster marked by an *arrow* in Figure 8*B*. *Arrows* in *B* point to clusters in the adult projection. Dorsal is *up*; medial is to the *right*. Scale bars, 200  $\mu\text{m}$ . *C*, Histogram indicating the area of MGN (including all its subdivisions) as a function of age. *D*, Histogram of the area of retinal projections to the MGN as a function of age. *E*, Histogram indicating the percentage of the MGN area innervated by retinal fibers as a function of age. *F*, Histogram of the percentage of retinal projections forming clusters (clustering index; see Materials and Methods) as a function of age. For number of animals analyzed in each developmental group, see Materials and Methods. Error bars indicate SEM.

both the MGN and the retinal projection zones grew at similar rates during this period (see above). However, between P22 and adulthood, the MGN continued to increase in size whereas the retino-MGN projection did not, so that the percentage of MGN invaded by retinal fibers decreased by approximately twofold ( $p < 0.05$ ; Fig. 11E).

Early in development, most of the retino-MGN projection was diffuse and showed little or no clustering until P8 (Fig. 11F). By the end of the third postnatal week, the clustering index (defined as the percentage of the retino-MGN projection area that is clustered) increased by approximately sevenfold ( $p = 0.003$ ). No significant changes in the clustering index were observed between the end of the third and of the fourth postnatal weeks or later ( $p > 0.05$ ).

**DISCUSSION**

In the present study, we have shown that retinal projections to the MGN in rewired ferrets are arranged in clusters that are scattered throughout the MGN subdivisions. Clusters arising from the ipsilateral eye are frequently apposed to, but spatially segregated from, clusters arising from the contralateral eye. Both clustering and eye-specific segregation in MGN arise as a refinement of initially diffuse and overlapped projections. Partial deafferentation of another novel retinal target, LP, also results in eye-specific clustering and segregation.

**Distribution, axon trajectories, and extent of novel retinothalamic projections**

The normal MGN is organized into several subnuclei (MGv, Po, MGd, MGm), each with a distinct cytoarchitectonic organization and a specific pattern of connections with the various auditory cortical fields (Winer et al., 1977; Imig and Morel, 1988; Winer, 1992). In the present study, we have observed that the MGN in rewired ferrets retains a normal cytoarchitectonic pattern in Nissl stain, and that retinal projections innervate mainly the rostral half

of the nucleus, terminating in all the MGN subdivisions. The rostral half of MGv sends a heavy projection to A1 and a sparser projection to the anterior field (A) in normal cats (Rose and Woolsey, 1949; Andersen et al., 1980; Imig and Morel, 1984; Morel and Imig, 1987) and ferrets (Pallas et al., 1990; Angelucci et al., 1993). A normal connectivity pattern between MGv and A1 is retained in rewired ferrets (Pallas et al., 1990). Thus, the anatomical substrate exists for visual A1 cells to be driven by the novel retino-MGN pathway.

In normal cats (Andersen et al., 1980; Morel and Imig, 1987) and ferrets (Angelucci, 1966), Po sends projections mainly to A, but also to A1. Projections from MGd predominantly reach the secondary auditory field (A2) and other nonprimary auditory areas, whereas projections from MGm are quite widespread, extending to each cortical auditory field (Winer et al., 1977; Morel and Imig, 1987). These anatomical data suggest that visual input might reach other auditory cortical fields in addition to A1, including field A and other auditory areas.

Retinal axons were found to enter the MGN from all around the nucleus, arising from the optic tract and the retinal targets that surround MGN, including the LGN and LP. This observation suggests that a diffusible trophic factor might be released by the auditory thalamus in response to the neonatal deafferentation. A similar phenomenon was observed in LP, which, however, is more abundantly reinnervated by retinal fibers than MGN. One possible explanation for the different extent of retinal innervation in LP and MGN is that proximity of growing axons to a potential terminal target determines whether and to what extent axons terminate in that target. In normal ferrets, the LP/Pulvinar is crossed by a large number of optic tract axons, directed to SC and PT. Partial LP deafferentation might induce reactive sprouting of these axons, which, because they are already passing through LP, might have a competitive advantage over other more distantly placed inputs. Moreover, in rewired ferrets, the caudal part of LP

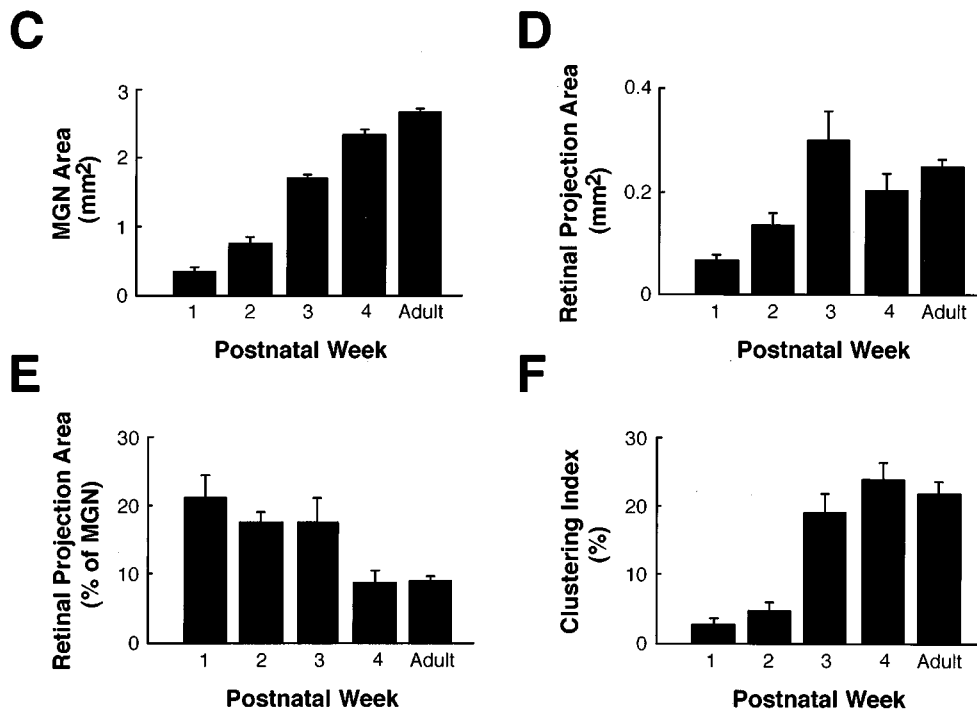
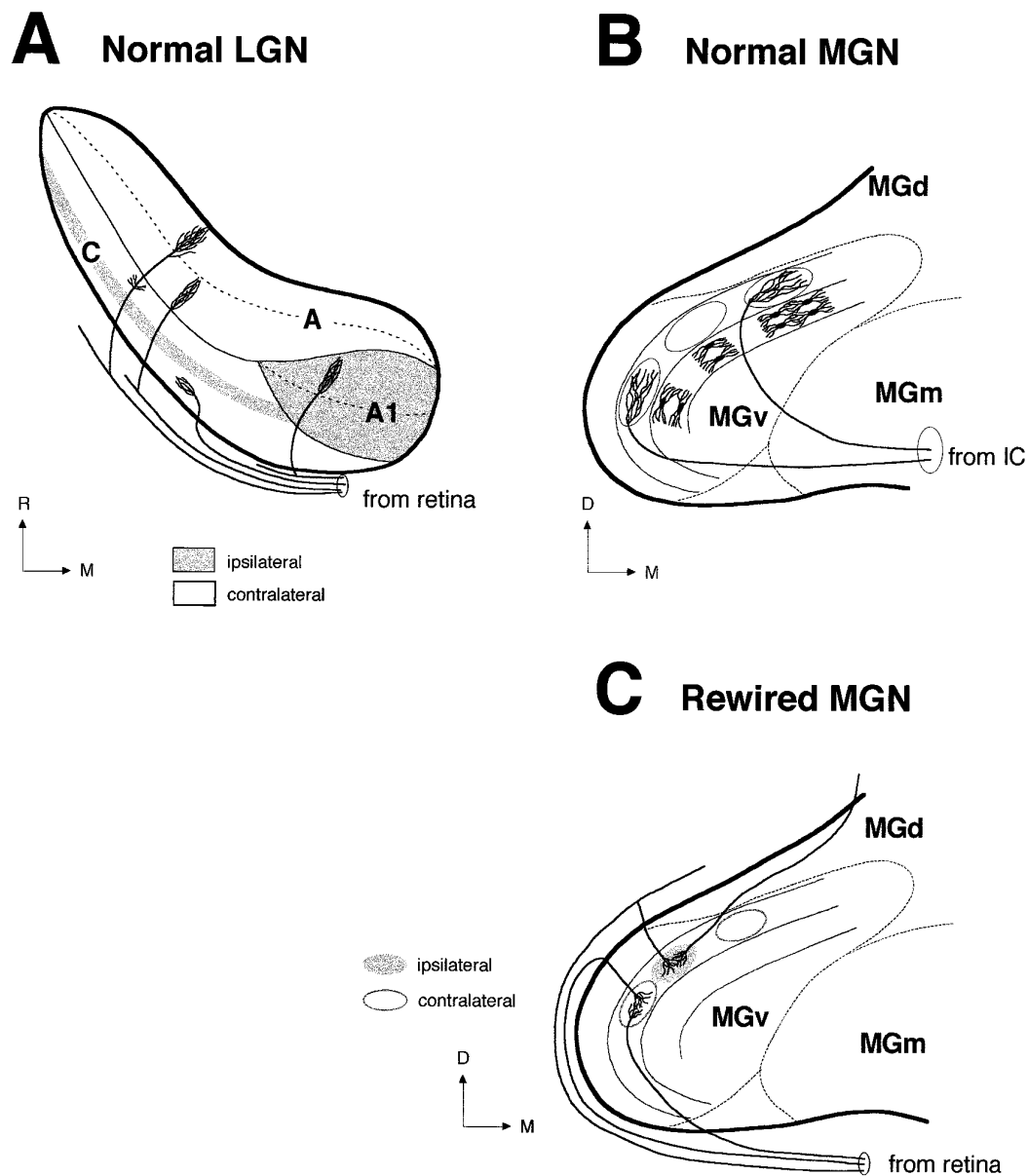


Figure 11 continued.



**Figure 12.** Terminal patterns of afferent projections to the normal LGN, normal MGv, and rewired MGv. *A*, Schematic representation of retinal projections to the normal ferret LGN in the horizontal plane. Projections from the ipsilateral (gray areas) and contralateral (empty areas) retinae segregate into eye-specific layers in the LGN (*A*, *A1*, *C*) (Linden et al., 1981). Within layers *A* and *A1*, afferent projections from the contralateral and ipsilateral eyes, respectively, further segregate into on-center and off-center sublayers (dashed lines) (Hahm et al., 1991). Three main morphological types of retinogeniculate axons have been described in the ferret LGN (Roe et al., 1989; Pallas et al., 1994): X axons project to the A layers, Y axons to the A and C layers, and W axons only to the C layers. *B*, Schematic representation of afferent projections from the IC to the normal MGv in the coronal plane. In MGv, projections from the IC form terminal clusters (ovals) aligned within dorsoventrally oriented fibrodendritic lamellae (Kudo and Niimi, 1980). The laminar pattern in MGv results from the ordered alignment of relay neurons (Morest, 1964, 1965; Winer, 1992). The position of the dendritic trees of these cells within a MGv lamina is illustrated (medial lamina). Axon arbors from the IC contribute to the laminar pattern of MGv by being elongated dorsoventrally (Morest, 1965) and anteroposteriorly (Pallas and Sur, 1994). *C*, Schematic representation of the novel retinal projection to MGv in the coronal plane. In rewired MGv, similar to the normal IC-to-MGv projection (*B*), retinal axons form terminal clusters aligned along lamellae. The lamellar organization of MGv is preserved in rewired ferrets (Pallas et al., 1990). However, similar to the normal retino-LGN projection (*A*), projections from the ipsilateral (gray oval) and contralateral (empty oval) retinae are segregated in MGv. Thus, segregation of retinal afferents occurs in the form of adjacent but nonoverlapping eye-specific clusters. Clusters are formed by the convergence and overlap of several axon arbors. Retino-MGN arbors are more restricted than IC-to-MGN arbors (compare *C* and *B*) (Pallas and Sur, 1994) and resemble in size W-cell axon arbors in the LGN and SC (Pallas et al., 1994). *A*, *A1*, *C*, Layers A, A1, and C of the LGN; *D*, dorsal; *M*, medial; *R*, rostral.

is mainly surrounded by retinal targets because the ventrally located auditory afferents to MGN have been extensively removed. Thus, other inputs to LP might also arise from the retinal targets surrounding this nucleus. In contrast, MGN in normal ferret kits is crossed by few optic tract axons and is surrounded by retinal as well as nonretinal targets and fiber tracts. Indeed, an

observation of the present study suggests that retinal axons in MGN might compete for terminal synaptic space with alternative inputs (see, for example, Crain and Hall, 1980a,b for a comparable conclusion regarding inputs to hamster LP after neonatal SC lesions). In adult rewired ferrets, MGN preserves its normal size, despite the extensive deafferentation performed at birth, but is

only partly reinnervated by retinal fibers. Experiments are currently under way to identify inputs innervating nonretinal recipient regions of the MGN in rewired ferrets.

### Clustering and eye-specific segregation of retino-MGN projections: specification by afferents and targets

Clustering of like inputs and their segregation from inputs of an opposite type are commonly observed in retinal projections to some normal targets, such as LGN and SC, and may depend on afferent activity. However, the specific pattern by which clustering and segregation occur varies in different retinal targets. Thus for example, the ferret retinogeniculate projection (Fig. 12A) segregates into parallel eye-specific layers (Linden et al., 1981) and on/off sublayers (Stryker and Zahs, 1983; Hahm and Sur, 1988; Hahm et al., 1991), whereas the retinocollicular projection segregates into a periodic pattern of eye-specific clusters (Zhang and Hoffmann, 1993). The generation of specific terminal patterns might depend on intrinsic features of the target. In the present study, we have addressed this issue by examining the resulting pattern of connections when inputs from the two eyes are redirected to novel targets, the cytological organization of which differs significantly from that of both SC and LGN. In the normal MGN, although the two ears are not represented separately, neurons in MGv (Fig. 12B) tuned to the same sound frequency segregate into thin laminae oriented dorsoventrally (isofrequency axis), and a systematic progression of sound frequencies occurs across the lateromedial dimension (tonotopic axis). In contrast, no ordered tonotopic organization has been detected in MGd or MGm (for review, see Winer, 1992). The laminar pattern in MGv is physiologically and anatomically analogous to the retinotopic arrangement of retinal axons in LGN and results from the ordered alignment of the typical MGv relay cells: the tufted neurons. These cells have characteristically elongated dendritic trees (Fig. 12B), oriented exclusively in the dorsoventral and rostrocaudal directions, with average diameters in the cat of 120  $\mu\text{m}$  (dorsoventral) and 22.5  $\mu\text{m}$  (mediolateral) (Morest, 1964, 1965; Majorossy and Kiss, 1976). Afferent fibers of the BIC contribute to the laminated pattern of MGv by terminating within a fibrodendritic lamina (Fig. 12B) and by contacting dendrites of adjacent laminae (Morest, 1965). Thus, in respect to individual fiber spread, a fibrodendritic lamina consists of 2 dendritic layers and is about 50–100  $\mu\text{m}$  wide (Winer, 1985). The laminar arrangement of relay cells in MGv of normal ferrets can be revealed by focal injection of retrograde tracers in A1 (F. Clascá, A. Angelucci, and M. Sur, unpublished observations) and is preserved in MGv of rewired ferrets (Pallas et al., 1990). Clusters of retino-MGN projections in MGv of rewired animals (Fig. 12C) seem to parallel the orientation of relay cell dendrites, being elongated dorsoventrally (mean size, 138  $\mu\text{m}$ ) and rostrocaudally (mean size, 151  $\mu\text{m}$ ), and to span approximately the width of a fibrodendritic lamina (mean width, 61–80  $\mu\text{m}$ ). In contrast, clusters in MGd and MGm, although often elongated, do not show any systematic orientation, consistent with the normal lack of orientation of dendritic trees in these subdivisions (Winer, 1985).

Another striking feature of rewired MGN is the alignment of retinal clusters along the isofrequency axis in MGv (Fig. 12C), but not in MGd or MGm. Studies in the cat (Kudo and Niimi, 1980) and bat (Wenstrup et al., 1994) have demonstrated that after injections of anterograde tracers in IC, terminal labeling in MGv appears as dense clusters of terminals aligned dorsoventrally, often forming “bands” (Fig. 12B). In contrast, in other subdivisions labeling consists of scattered “patches,” consistent with the

normal lack of a laminar pattern in these subdivisions. Thus, the overall pattern of retino-MGv projections (Fig. 12C) resembles the normal pattern of IC-to-MGv afferents (Fig. 12B). Similarly, the terminal slabs formed by retino-LP afferents in rewired animals resemble the slab-like pattern of normal tectal projections to the cat LP (Graybiel, 1972; Graybiel and Berson, 1980). Together, the above observations suggest that the novel target restricts or defines the shape, size, and distribution of terminal retinal clusters. Consistent with our observations, previous studies of retinal projections to the hamster MGN and ventrobasal nucleus (Campbell and Frost, 1987, 1988) have shown that at the ultrastructural level, synaptic morphology seems to be controlled by intrinsic features of the target. At the same time, sizes of individual retino-MGN arbors that contribute to terminal clusters resemble arbors of retinal W-cell axons in the LGN and SC (Pallas et al., 1994) and are smaller than arbors of X- and Y-cell axons in the LGN (Roe et al., 1989).

If the shape and size of clusters are constrained by the target, clustering per se, and eye-specific segregation of clusters in the novel targets, are more likely to be regulated by afferents or by interactions between afferents and their target cells. This hypothesis is suggested by previous evidence for activity-dependent sorting of retinal afferents to LGN (Shatz and Stryker, 1988; Sretavan et al., 1988; Hahm et al., 1991) and SC (for review, see White and Chalupa, 1991). In most mammals, retinal afferents segregate into eye-specific domains in the LGN (Guillery, 1970; Hickey and Guillery, 1974; Linden et al., 1981) and SC (Graybiel, 1975; Chalupa and Rhoades, 1979; Lund et al., 1980; Hoffmann et al., 1984; Illing, 1989; Murphy et al., 1992). During development of retinogeniculate (So et al., 1978; Linden et al., 1981; Shatz, 1983; Sretavan and Shatz, 1986) and retinocollicular (Frost et al., 1979; Land and Lund, 1979; Williams and Chalupa, 1982; Thompson, 1990) afferents, eye-specific segregation has been shown to occur as a refinement of initially diffuse and interspersed projections by a process dependent on afferent activity (for the LGN: Shatz and Stryker, 1988; for review, see Shatz, 1990; for the SC: Lund et al., 1973, 1980; Finlay et al., 1979; Insausti et al., 1984; Jen et al., 1984). Moreover, eye-specific segregation in a target that normally does not receive projections from both eyes has been shown to occur in the optic tectum of embryonically created three-eyed frogs (Constantine-Paton and Law, 1978; Law and Constantine-Paton, 1981) and to be dependent both on presynaptic (Reh and Constantine-Paton, 1985) and postsynaptic (Cline et al., 1987) activity. In the present study, we have shown that clustering and eye-specific segregation of retinal afferents occur also in nonretinal targets, and that their emergence involves a significant progressive remodeling of axon arbors, similar to that described for the emergence of retinal termination patterns within the LGN. In addition, this remodeling in MGN occurs over the same time period as the formation of eye-specific layers and on/off sublayers in the ferret LGN (Hahm et al., 1991), suggesting that these processes may share similar afferent-driven mechanisms.

### REFERENCES

- Andersen RA, Knight PL, Merzenich MM (1980) The thalamocortical and corticothalamic connections of AI, AII, and the anterior auditory field (AAF) in the cat: evidence for two largely segregated systems of connections. *J Comp Neurol* 194:663–701.
- Angelucci A (1996) Experimental retinal projections to the auditory thalamus: morphology, development and effects on auditory cortical organization. PhD thesis, Massachusetts Institute of Technology.
- Angelucci A, Clascá F, Sur M (1993) Multiple cortical auditory fields in the ferret defined by their architectonics and thalamocortical connections. *Neurosci Abstr* 19:1427.

- Angelucci A, Clascá F, Sur M (1994) Retinal projections induced into the auditory thalamus in ferrets: differential terminal distribution and eye-specific zones. *Soc Neurosci Abstr* 20:1107.
- Angelucci A, Cramer KS, Sur M (1995) Emergence of clustered eye-specific patterns in experimentally induced retinal projections to the ferret auditory thalamus. *Soc Neurosci Abstr* 21:1307.
- Angelucci A, Bricolo E, Sur M (1996a) Development of experimentally induced retinal projections to the ferret auditory thalamus: a quantitative study. *Soc Neurosci Abstr* 22:1730.
- Angelucci A, Clascá F, Sur M (1996b) Anterograde axonal tracing with the subunit B of cholera toxin: a highly sensitive immunohistochemical protocol for revealing fine axonal morphology in adult and neonatal brains. *J Neurosci Methods* 65:101–112.
- Bear MF, Kleinschmidt A, Gu Q, Singer W (1990) Disruption of experience-dependent synaptic modifications in striate cortex by infusion of an NMDA receptor antagonist. *J Neurosci* 10:909–925.
- Benedek G, Norita M, Creutzfeldt OD (1983) Electrophysiological and anatomical demonstration of an overlapping striate and tectal projection to the lateral posterior-pulvinar complex of the cat. *Exp Brain Res* 52:157–169.
- Caldwell RB, Mize RR (1981) Superior colliculus neurons which project to the cat lateral posterior nucleus have varying morphologies. *J Comp Neurol* 203:53–66.
- Calford MB, Aitkin LM (1983) Ascending projections to the medial geniculate body of the cat: evidence for multiple, parallel auditory pathways through the thalamus. *J Neurosci* 3:2365–2380.
- Campbell G, Frost DO (1987) Target-controlled differentiation of axon terminals and synaptic organization. *Proc Natl Acad Sci USA* 84:6929–6933.
- Campbell G, Frost DO (1988) Synaptic organization of anomalous retinal projections to the somatosensory and auditory thalamus: target-controlled morphogenesis of axon terminals and synaptic glomeruli. *J Comp Neurol* 272:383–408.
- Chalupa LM, Rhoades RW (1979) An autoradiographic study of the retinotectal projection in the golden hamster. *J Comp Neurol* 186:561–570.
- Cline HT, Debski EA, Constantine-Paton M (1987) *N*-Methyl-D-aspartate receptor antagonist desegregates eye-specific stripes. *Proc Natl Acad Sci USA* 84:4342–4345.
- Constantine-Paton M, Law MI (1978) Eye-specific termination bands in tecta of three-eyed frogs. *Science* 202:639–641.
- Crain BJ, Hall WC (1980a) The organization of the lateral posterior nucleus of the golden hamster after neonatal superior colliculus lesions. *J Comp Neurol* 193:383–401.
- Crain BJ, Hall WC (1980b) The organization of afferents to the lateral posterior nucleus in the golden hamster after different combinations of neonatal lesions. *J Comp Neurol* 193:403–412.
- Cramer KS, Sur M (1995) Activity-dependent remodeling of connections in the mammalian visual system. *Curr Opin Neurobiol* 5:106–111.
- Cramer KS, Sur M (1997) Blockade of afferent impulse activity disrupts ON/OFF sublamination in the ferret lateral geniculate nucleus. *Dev Brain Res*, in press.
- Finlay BL, Wilson KG, Schneider GE (1979) Anomalous ipsilateral retinotectal projections in Syrian hamsters with early lesions: topography and functional capacity. *J Comp Neurol* 183:721–740.
- Frost DO (1981) Orderly anomalous retinal projections to the medial geniculate, ventrobasal, and lateral posterior nuclei of the hamster. *J Comp Neurol* 203:227–256.
- Frost DO (1982) Anomalous visual connections to somatosensory and auditory systems following brain lesions in early life. *Dev Brain Res* 3:627–635.
- Frost DO (1986) Development of anomalous retinal projections to non-visual thalamic nuclei in syrian hamsters: a quantitative study. *J Comp Neurol* 252:95–105.
- Frost DO, So K-F, Schneider GE (1979) Postnatal development of retinal projections in Syrian hamsters: a study using autoradiographic and anterograde degeneration techniques. *Neuroscience* 4:1649–1677.
- Garraghty PE, Shatz CJ, Sur M (1988a) Prenatal disruption of binocular interactions creates novel lamination in the cat's lateral geniculate nucleus. *Vis Neurosci* 1:93–102.
- Garraghty PE, Shatz CJ, Sretavan DW, Sur M (1988b) Axon arbors of X and Y retinal ganglion cells are differentially affected by prenatal disruption of binocular inputs. *Proc Natl Acad Sci USA* 85:7361–7365.
- Graham J (1977) An autoradiographic study of the efferent connections of the superior colliculus in the cat. *J Comp Neurol* 173:629–654.
- Graybiel AM (1972a) Some extrageniculate visual pathways in the cat. *Invest Ophthalmol* 11:322–332.
- Graybiel AM (1972b) Some fiber pathways related to the posterior thalamic region in the cat. *Brain Behav Evol* 6:363–393.
- Graybiel AM (1975) Anatomical organization of the retinotectal afferents in the cat: an autoradiographic study. *Brain Res* 96:1–23.
- Graybiel AM, Berson DM (1980) Histochemical identification and afferent connections of subdivisions in the lateralis posterior-pulvinar complex and related thalamic nuclei in the cat. *Neuroscience* 5:1175–1238.
- Guillery RW (1970) The laminar distribution of retinal fibers in the dorsal lateral geniculate nucleus of the cat: a new interpretation. *J Comp Neurol* 138:339–368.
- Hahm J-O, Sur M (1988) The development of individual retinogeniculate axons during laminar and sublaminar segregation in the ferret LGN. *Soc Neurosci Abstr* 14:460.
- Hahm J-O, Langdon RB, Sur M (1991) Disruption of retinogeniculate afferent segregation by antagonists to NMDA receptors. *Nature* 351:568–570.
- Hata Y, Stryker MP (1994) Control of thalamocortical afferent rearrangement by postsynaptic activity in developing visual cortex. *Science* 265:1732–1735.
- Hickey TL, Guillery RW (1974) An autoradiographic study of retinogeniculate pathways in the cat and fox. *J Comp Neurol* 156:239–254.
- Hoffmann K-P, Ballas I, Wagner H-J (1984) Double labeling of retinofugal projections in the cat: a study using anterograde axonal transport of <sup>3</sup>H-proline and horseradish peroxidase. *Exp Brain Res* 53:420–430.
- Illing R-B (1989) The mosaic of the uncrossed retinal projections in the superior colliculus of the cat. *Exp Brain Res* 74:641–644.
- Imig TJ, Morel A (1984) Topographic and cytoarchitectonic organization of thalamic neurons related to their targets in low-, middle-, and high-frequency representations in cat auditory cortex. *J Comp Neurol* 227:511–539.
- Imig TJ, Morel A (1988) Organization of the cat's auditory thalamus. In: *Auditory function. Neurobiological basis of hearing* (Edelman GM, Gall WE, Cowan WM, eds), pp 457–484. New York: Wiley.
- Insausti R, Blakemore C, Cowan WM (1984) Ganglion cell death during development of ipsilateral retinocollicular projection in golden hamster. *Nature* 308:362–365.
- Jen LS, So K-F, Woo HH (1984) An anterograde HRP study of the retinocollicular projection in normal hamsters and hamsters with one eye enucleated at birth. *Brain Res* 294:169–173.
- Kalil RE, Schneider ER (1975) Abnormal synaptic connections of the optic tract in the thalamus after midbrain lesions in newborn hamsters. *Brain Res* 100:690–698.
- Kawamura S, Fukushima N, Hattori S, Kudo M (1980) Laminar segregation of cells of origin of ascending projections from the superficial layers of the superior colliculus in the cat. *Brain Res* 184:486–490.
- Kudo M, Niimi K (1980) Ascending projections of the inferior colliculus in the cat: an autoradiographic study. *J Comp Neurol* 191:545–556.
- Land PW, Lund RD (1979) Development of the rat's uncrossed retinotectal pathway and its relation to plasticity studies. *Science* 205:698–700.
- Law MI, Constantine-Paton M (1981) Anatomy and physiology of experimentally produced striped tecta. *J Neurosci* 1:741–759.
- Law MI, Zahs KR, Stryker MP (1988) Organization of primary visual cortex (area 17) in the ferret. *J Comp Neurol* 278:157–180.
- Linden DC, Guillery RW, Cucchiari J (1981) The dorsal lateral geniculate nucleus of the normal ferret and its postnatal development. *J Comp Neurol* 203:189–211.
- Lund RD, Cunningham TS, Lund JS (1973) Modified optic pathways after unilateral eye removal in young rats. *Brain Behav Evol* 8:51–72.
- Lund RD, Land PW, Boles J (1980) Normal and abnormal uncrossed retinotectal pathways in rats: an HRP study in adults. *J Comp Neurol* 189:711–720.
- Majorossy K, Kiss A (1976) Specific patterns of neuron arrangement and of synaptic articulation in the medial geniculate body. *Exp Brain Res* 26:1–17.
- McIlwain JT (1978) Properties of cells projecting rostrally from the superficial layers of the cat's superior colliculus. *Brain Res* 143:445–457.
- Mesulam MM (1978) Tetramethyl benzidine for horseradish peroxidase neurohistochemistry: a non-carcinogenic blue reaction product with superior sensitivity for visualizing neural afferents and efferents. *J Histochem Cytochem* 26:106–117.
- Morel A, Imig TJ (1987) Thalamic projections to fields A, AI, P, and VP in the cat auditory cortex. *J Comp Neurol* 265:119–144.

- Morest DK (1964) The neuronal architecture of the medial geniculate body of the cat. *J Anat* 98:611–630.
- Morest DK (1965) The laminar structure of the medial geniculate body of the cat. *J Anat* 99:143–160.
- Morest DK, Winer JA (1986) The comparative anatomy of neurons: homologous neurons in the medial geniculate body of the opossum and the cat. *Adv Anat Embryol Cell Biol* 97:1–96.
- Murphy KM, Jones DJ, Van Sluyters RC (1992) Ocular dominance columns in cat superior colliculus. *Invest Ophthalmol Vis Sci Abstr* 33:1214.
- Pallas SL, Sur M (1994) Morphology of retinal axon arbors induced to arborize in a novel target, the medial geniculate nucleus. II. Comparison with axons from the inferior colliculus. *J Comp Neurol* 349:363–376.
- Pallas SL, Roe AW, Sur M (1990) Visual projections induced into the auditory pathway of ferrets. I. Novel inputs to primary auditory cortex (AI) from the LP/pulvinar complex and the topography of the MGN-AI projection. *J Comp Neurol* 298:50–68.
- Pallas SL, Hahm J, Sur M (1994) Morphology of retinal axons induced to arborize in a novel target, the medial geniculate nucleus. I. Comparison with arbors in normal targets. *J Comp Neurol* 349:343–362.
- Reh TA, Constantine-Paton M (1985) Eye-specific segregation requires neural activity in the three-eyed *Rana pipiens*. *J Neurosci* 5:1132–1143.
- Roe AW, Garraghty PE, Sur M (1989) Terminal arbors of single ON-center and OFF-center retinal ganglion cell axons within the ferret's lateral geniculate nucleus. *J Comp Neurol* 228:208–242.
- Roe AW, Garraghty PE, Esguerra M, Sur M (1993) Experimentally induced visual projections to the auditory thalamus: evidence for a W cell pathway. *J Comp Neurol* 334:263–280.
- Rose JE, Woolsey CN (1949) The relations of thalamic connections, cellular structure, and evocable electrical activity in the auditory region of the cat. *J Comp Neurol* 91:441–466.
- Schneider GE (1973) Early lesions of superior colliculus: factors affecting the formation of abnormal retinal projections. *Brain Behav Evol* 8:73–109.
- Shatz CJ (1983) The prenatal development of the cat's retinogeniculate pathway. *J Neurosci* 3:482–499.
- Shatz CJ (1990) Impulse activity and the patterning of connections during CNS development. *Neuron* 5:745–756.
- Shatz CJ, Stryker MP (1988) Prenatal tetrodotoxin infusion blocks segregation of retinogeniculate afferents. *Science* 242:87–89.
- Smetters DK, Hahm J-O, Sur M (1994) An *N*-methyl-D-aspartate receptor antagonist does not prevent eye-specific segregation in the ferret retinogeniculate pathway. *Brain Res* 658:168–178.
- So K-F, Schneider GE, Frost DO (1978) Postnatal development of retinal projections to the lateral geniculate body in Syrian hamsters. *Brain Res* 142:343–352.
- Sretavan DW, Shatz CJ (1986) Prenatal development of retinal ganglion cell axons: segregation into eye-specific layers within the cat's lateral geniculate nucleus. *J Neurosci* 6:234–251.
- Sretavan DW, Shatz CJ, Stryker MP (1988) Modification of retinal ganglion cell axon morphology by prenatal infusion of tetrodotoxin. *Nature* 336:468–471.
- Stryker MP, Harris W (1986) Binocular impulse blockade prevents the formation of ocular dominance columns in cat visual cortex. *J Neurosci* 6:2117–2133.
- Stryker MP, Zaks K (1983) ON and OFF sublaminae in the lateral geniculate nucleus of the ferret. *J Neurosci* 3:1943–1951.
- Sur M, Garraghty PE, Roe AW (1988) Experimentally induced visual projections into auditory thalamus and cortex. *Science* 242:1437–1441.
- Thompson ID (1990) Retinal pathways and the developmental basis of binocular vision. In: *Vision: coding and efficiency* (Blakemore C, ed), pp 209–223. Cambridge: Cambridge UP.
- Wenstrup JJ, Larue DT, Winer JA (1994) Projections of physiologically defined subdivisions of the inferior colliculus in the mustached bat: targets in the medial geniculate body and extrathalamic nuclei. *J Comp Neurol* 346:207–236.
- White CA, Chalupa LM (1991) Development of mammalian retinofugal pathways. In: *Neuroanatomy of the visual pathways and their development* (Dreher B, Robinson SR, eds), pp 129–149. London: Macmillan.
- Williams RW, Chalupa LM (1982) Prenatal development of retinocollicular projections in the cat: an anterograde tracer transport study. *J Neurosci* 2:604–622.
- Winer JA (1985) The medial geniculate body of the cat. *Adv Anat Embryol Cell Biol* 86:1–98.
- Winer JA (1992) The functional architecture of the medial geniculate body and the primary auditory cortex. In: *The mammalian auditory pathway: neuroanatomy* (Webster DD, Popper AN, Fay RR, eds), pp 222–409. New York: Springer.
- Winer JA, Diamond IT, Raczkowski D (1977) Subdivisions of the auditory cortex of the cat: the retrograde transport of horseradish peroxidase to the medial geniculate body and posterior thalamic nuclei. *J Comp Neurol* 176:387–418.
- Zaks KR, Stryker MP (1988) Segregation of ON and OFF afferents to ferret visual cortex. *J Neurophysiol* 59:1410–1429.
- Zhang HY, Hoffmann K-P (1993) Retinal projections to the pretectum, accessory optic system and superior colliculus in pigmented and albino ferrets. *Eur J Neurosci* 5:486–500.